ANNUAL REVIEWS

Annual Review of Biochemistry

Structure and Mechanisms of F-Type ATP Synthases

Werner Kühlbrandt

Department of Structural Biology, Max Planck Institute of Biophysics, 60438 Frankfurt, Germany; email: werner.kuehlbrandt@biophys.mpg.de

Annu. Rev. Biochem. 2019. 88:515–49

First published as a Review in Advance on March 22, 2019

The *Annual Review of Biochemistry* is online at biochem.annualreviews.org

https://doi.org/10.1146/annurev-biochem-013118-110903

Keywords

membrane protein structure, electron cryo-microscopy, cryo-EM, proton channels, mitochondria, chloroplasts, proton-motive force, ATP synthase dimers

Abstract

F_1F_o ATP synthases produce most of the ATP in the cell. F-type ATP synthases have been investigated for more than 50 years, but a full understanding of their molecular mechanisms has become possible only with the recent structures of complete, functionally competent complexes determined by electron cryo-microscopy (cryo-EM). High-resolution cryo-EM structures offer a wealth of unexpected new insights. The catalytic F_1 head rotates with the central γ-subunit for the first part of each ATP-generating power stroke. Joint rotation is enabled by subunit *δ/OSCP* acting as a flexible hinge between F_1 and the peripheral stalk. Subunit *a* conducts protons to and from the *c*-ring rotor through two conserved aqueous channels. The channels are separated by ∼6 Å in the hydrophobic core of F_o, resulting in a strong local field that generates torque to drive rotary catalysis in F_1. The structure of the chloroplast F_1F_o complex explains how ATPase activity is turned off at night by a redox switch. Structures of mitochondrial ATP synthase dimers indicate how they shape the inner membrane cristae. The new cryo-EM structures complete our picture of the ATP synthases and reveal the unique mechanism by which they transform an electrochemical membrane potential into biologically useful chemical energy.

Contents

INTRODUCTION

ATP synthases are macromolecular turbines that convert the energy inherent in a transmembrane electrochemical gradient into the energy of a covalent phosphoanhydride bond. This is the only known mechanism by which living organisms can transduce a membrane potential directly into biologically useful chemical energy, and the reaction is one of the most fundamental—arguably the most fundamental—in biology.

ATP synthases make adenosine triphosphate (ATP), the universal energy currency in the cell, from adenosine diphosphate (ADP) and inorganic phosphate (P_i) by rotary catalysis, a process common to all forms of life. Rotary ATPases include the F-type ATPases of bacteria, mitochondria and chloroplasts (1–3). They are termed F-type because they were originally known as coupling factors (CFs) that couple ATP synthesis to electron and proton transport reactions of the mitochondrial or bacterial respiratory chain (4, 5). Later the "C" was dropped to avoid confusion with the chloroplast ATPase, which is often referred to as cF_1F_o. Because of their central role in bioenergetics and cell metabolism, ATP synthases have been studied intensely by biochemists, molecular biologists, biophysicists, and structural biologists ever since their discovery in the 1960s (4). In 1997, Paul Boyer and John Walker were awarded the Nobel Prize in Chemistry for unraveling the catalytic mechanism of ATP synthesis (jointly with Jens Skou for his pioneering work on the unrelated P-type ATPases). A number of excellent and comprehensive reviews summarize previous work on rotary catalysis and X-ray structures of key ATP synthase components (1–3, 6–9).

Rotary ATPases also include the eukaryotic vacuolar (V-type) ATPases (10) and the A-type ATPases (11) of archaea and some extremophilic bacteria. In vitro, all are fully reversible. Either they use an electrochemical gradient to produce ATP from ADP and phosphate in ATP synthesis mode or, in the reverse ATP hydrolysis mode, they create such a gradient, using the energy released by ATP hydrolysis to pump protons across the membrane. In vivo, mitochondrial and chloroplast ATP synthases operate only in synthesis mode, whereas bacterial F-type ATPases work in either direction, depending on growth conditions. V-type ATPases hydrolyze ATP to acidify intracellular compartments such as synaptic vesicles (12) or the central vacuole of yeast cells (13). A-type ATPases generate ATP from a proton gradient like the F-type but may also work as ATP-driven ion pumps like the V-type (14), to which they are more closely related. This review focuses on recent progress in understanding the structure and mechanisms of F-type ATPases. Most of the structures that provided new insights were obtained by electron cryo-microscopy (cryo-EM).

Within the past five years, cryo-EM has made extraordinary progress, described as a resolution revolution (15). For decades, high-resolution structure determination of biological macromolecules was the prerogative of X-ray crystallography or NMR spectroscopy. Only in special cases, such as highly symmetrical icosahedral viruses (16, 17) and multienzyme complexes (18), or with well-ordered 2D crystals of membrane proteins (19–21) had it been possible to determine structures by cryo-EM at a resolution that enabled amino acid side chains to be fitted and reliable atomic models to be built. This all changed with the introduction of direct electron detectors that record high-resolution electron micrographs of radiation-sensitive biological samples (22), and the simultaneous development of powerful image processing software to extract the high-resolution information from the micrographs (23). At the same time, the mechanical and optical stability of electron microscopes had improved to the point at which it became possible to collect images of single, unstained biological macromolecules at near-atomic resolution. As the combined result of these developments, high-resolution structures of proteins and protein complexes above a certain minimal size (currently 60 to 80 kDa) can now be determined without crystals by cryo-EM, at a rate that could not be imagined a few years ago.

The resolution revolution in cryo-EM is having a major impact on the study of large membrane protein complexes that are either too unstable or too dynamic for X-ray crystallography. Rotary ATPases are by their very nature dynamic, and they tend to be unstable in detergent solution. Intact rotary ATPases have resisted crystallization for almost 40 years. To date, no high-resolution X-ray structure of a complete ATP synthase has been reported. However, a number of key components have been crystallized and their structures determined by X-ray crystallography (24–27). Fitted into earlier low-resolution cryo-EM envelopes (28), the components yielded mosaic models that went a long way toward explaining how the whole assembly works. Yet, essential elements of the mechanism, especially the structural basis of proton translocation and how it drives ATP synthesis, remained intractable. These central aspects have become clear only now with the recent high-resolution cryo-EM structures of intact, functionally competent ATP synthases (**Table 1**).

Cryo-EM not only delivers high-resolution details of isolated proteins or complexes by single-particle analysis. Electron cryo-tomography (cryo-ET), another powerful application of cryo-EM, reveals their structures in a cellular or organellar context by subtomogram averaging, usually—but not necessarily (29)—at lower resolution. Recent cryo-ET studies have changed our perception of how F-type ATPases are arranged in mitochondrial and chloroplast membranes.

OVERALL ORGANIZATION OF F-TYPE ATPases

F-type ATPases are large, 550- to 1,600-kDa membrane protein complexes (**Table 2**) that all conform to the same basic building plan (**Figure 1**). They consist of two principal parts, the spherical

Table 1 Recent cryo-EM structures of F-type ATP synthases

Species	*Escherichia coli*	Spinach	*Yarrowia lipolytica*	*Saccharomyces cerevisiae*	*Saccharomyces cerevisiae*	Bovine heart	*Polytomella* sp.
ATP synthase type	Bacterial	Chloroplast	Mitochondrial	Mitochondrial	Mitochondrial	Mitochondrial	Mitochondrial
Oligomeric state	F_1F_o monomer	cF_1F_o monomer	mtF_1F_o dimer	mtF_1F_o half dimer	mtF_o dimer	mtF_1F_o half dimer	mtF_1F_o dimer
Dimer type	NA	NA	Type I	Type I	Type I	Type I	Type II
PDB access codes (atomic coordinates)	5T4O	6FKF, 6FKH, 6FKI	5FL7	6CP3, 6CP5–6CP7	6B2Z	5ARA–5ARI, 5FIJ–5FIL	6RD5–6REU
EMDB access codes (cryo-EM map)	9345, 9346, 9348, 20006–20008	4270–4273	8151	7546–7549	7037	3164–3170	4806–4857
Resolution (Å)	5.0–5.5	2.9–3.4	6.2	3.6–3.8	3.6	6.4 to 7.4	2.7–2.8
Reference(s)	46a	48	79	76	78	75	80, 81

Abbreviations: ATP, adenosine triphosphate; cryo-EM, electron cryo-microscopy; EMDB, Electron Microscopy Data Bank; NA, not applicable; PDB, Protein Data Bank.

F_1 head—so called because of its conspicuous globular shape in early electron micrographs (4, 30)—and the F_o subcomplex in the membrane. The F_1 head measures approximately 8 nm in diameter, extends approximately 11 nm above the membrane surface, and is the site of ATP synthesis. The F_o complex renders mitochondrial ATPases sensitive to inhibition by the antibiotic oligomycin, hence the subscript (4).

The F_1 head is an assembly of three α- and three β-subunits, arranged in near-three-fold symmetry around the central γ-subunit. Each F_1 head has three active sites—β_E, β_{DP}, and β_{TP}—at the interface between β- and α-subunits (24). The catalytic nucleotide binding pockets are defined mostly by the β-subunits, with an essential arginine residue contributed by the α-subunits. In the binding-change mechanism discovered by Boyer et al. (7), the sites alternate from being empty (β_E) to being occupied by Mg-ADP and phosphate (β_{DP}), which are condensed to form Mg-ATP (β_{TP}) in synthesis mode. Polypeptide sequences and structures of the α-/β-subunits are similar, but the α-subunits each bind a structural Mg-ATP that does not participate in the catalytic cycle.

While the F_1 head produces or hydrolyzes ATP, the F_o motor generates torque (in synthesis mode) or pumps protons across the membrane (in hydrolysis mode). The signature components of the F_o motor are the *a*-subunit and a rotor ring of 8 to 17 *c*-ring subunits. F_o is connected to F_1 by the central stalk and one peripheral stalk (31). The central stalk of subunits γ, ε, and, in mitochondria, δ transmits torque generated by F_o to the catalytic F_1 head. The γ-subunit is firmly attached to the F_o rotor and acts as a crankshaft, forcing the α-/β-subunits into different conformations with different binding affinities for ATP or ADP and phosphate. A subunit termed δ in chloroplasts and bacteria (but *OSCP* in mitochondria) connects the peripheral stalk to F_1, preventing idle rotation of the catalytic head with F_o. Bacterial and chloroplast ATP synthases are structurally similar and comparatively simple, consisting of a minimal set of subunits (**Table 2**), whereas the subunit composition and peripheral stalk structures of mitochondrial ATP synthases are more complex and variable.

BACTERIAL ATP SYNTHASES

Under aerobic growth conditions, bacteria produce most of their ATP by an F-type ATPase in the cytoplasmic (inner) membrane. Under anaerobic conditions, they generate ATP by glycolysis and fermentation. The ATPase then works as an ATP-driven ion pump to generate the indispensable membrane potential. With few exceptions, bacterial F-type ATPases are proton-driven, although

Table 2 Protein subunits in cryo-EM structures of bacterial, chloroplast, and mitochondrial F-type ATP synthases

				Escherichia coli bacterial F_1F_o		Spinach chloroplast F_1F_o		*Saccharomyces cerevisiae* mitochondrial F_1F_o		Bovine heart mitochondrial F_1F_o		*Polytomella* sp. mitochondrial F_1F_o dimer	
Subunit name	**F_1F_o type**	**Gene (*S. cerevisiae*)**	**Primary function**	**Copies**	**Residues**	**Copies**	**Residues**	**Copies**	**Residues**	**Copies**	**Residues**	**Copies**	**Residues**
F_1 head													
α	All	*ATP1*	Structural, catalytic	3	513	3	507	3	510	3	510	6	524
β	All	*ATP2*	Catalytic	3	471	3	486	3	478	3	482	6	547
Central stalk													
γ	All	*ATP3*	Torque transmission	1	287	1	321	1	278	1	273	2	281
δ	mt	*ATP16*	Connection to *c*-ring	NE	NE	NE	NE	1	61	1	50	2	152
ε	mt	*ATP15*	Connection to *c*-ring	NE	NE	NE	NE	1	138	1	146	2	73
ε	bact, chl	NE	Autoinhibitory (in bacteria)	1	139	1	131	NE	NE	NE	NE	NE	NE
Peripheral stalk													
b	All	*ATP4*	Stator, F_1–F_o link	2	155	1	160	1	209	1	174	NE	NE
b′	bact, chl	NE	Stator, F_1–F_o link	NE	NE	1	143	NE	NE	NE	NE	NE	NE
δ	bact, chl	NE	Flexible hinge	1	177	1	179	NE	NE	NE	NE	NE	NE
OSCP	mt	*ATP5*	Flexible hinge	NE	NE	NE	NE	1	195	1	190	2	197
d	mt	*ATP7*	Structural	NE	NE	NE	NE	1	173	1	124	NE	NE
h (*F6*)	mt	*ATP14*	Structural	NE	NE	NE	NE	1	92	1	77	NE	NE
F_o motor													
a	All	*ATP6*	Stator, proton half channels	1	271	1	223	1	249	1	217	2	233
c	All	*ATP9*	Rotor, proton translocation	10	79	14	79	10	76	8	72	20	74
Type I dimer–specific subunits													
e	mt	*ATP21* (*TIM11*)	Dimer stability	NE	NE	NE	NE	1	49	1	ND	NE	NE
g	mt	*ATP20*	Dimer stability	NE	NE	NE	NE	1	106	1	ND	NE	NE
f	mt	*ATP17*	Structural	NE	NE	NE	NE	1	95	1	ND	NE	NE
j (*i,6.8PL*)	mt	*ATP18*	Structural	NE	NE	NE	NE	1	59	1	ND	NE	NE
k (*DAPIT*)	mt	*ATP19*	Dimer stability	NE	NE	NE	NE	1	68	1	ND	NE	NE
8 (*A6L*)	mt	*ATP8*	Structural	NE	NE	NE	NE	1	48	1	ND	NE	NE

(*Continued*)

Table 2 (*Continued*)

				Escherichia coli bacterial F_1F_o		Spinach chloroplast F_1F_o		*Saccharomyces cerevisiae* mitochondrial F_1F_o		Bovine heart mitochondrial F_1F_o		*Polytomella* sp. mitochondrial F_1F_o dimer	
Subunit name	**F_1F_o type**	**Gene (*S. cerevisiae*)**	**Primary function**	**Copies**	**Residues**	**Copies**	**Residues**	**Copies**	**Residues**	**Copies**	**Residues**	**Copies**	**Residues**
Type II dimer–specific subunits													
ASA1	mt	NE	Structural, dimer contact	NE	NE	NE	NE	NE	NE	NE	NE	2	618
ASA2	mt	NE	Structural	NE	NE	NE	NE	NE	NE	NE	NE	2	446
ASA3	mt	NE	Structural	NE	NE	NE	NE	NE	NE	NE	NE	2	252
ASA4	mt	NE	Structural	NE	NE	NE	NE	NE	NE	NE	NE	2	294
ASA5	mt	NE	Structural	NE	NE	NE	NE	NE	NE	NE	NE	2	123
ASA6	mt	NE	Structural, proton channel	NE	NE	NE	NE	NE	NE	NE	NE	2	124
ASA7	mt	NE	Structural	NE	NE	NE	NE	NE	NE	NE	NE	2	176
ASA8	mt	NE	Structural	NE	NE	NE	NE	NE	NE	NE	NE	2	89
ASA9	mt	NE	Structural	NE	NE	NE	NE	NE	NE	NE	NE	2	96
ASA10	mt	NE	Dimer contact	NE	NE	NE	NE	NE	NE	NE	NE	2	82
Totals													
Total residues					4,926		5,242		5,544		4,803*		14,378
Estimated total mass (kDa)					542		577		610		528*		1,581

For *E. coli*, *S. cerevisiae*, and bovine mitochondrial ATP synthase, the number of residues in each subunit is taken from the genomic sequence. For chloroplast and *Polytomella* ATP synthase, the number refers to the residues in the atomic model.

Abbreviations: *, without dimer-specific subunits; bact, bacterial; chl, chloroplast; cryo-EM, electron cryo-microscopy; mt, mitochondrial; ND, atomic structure not determined; NE, nonexistent.

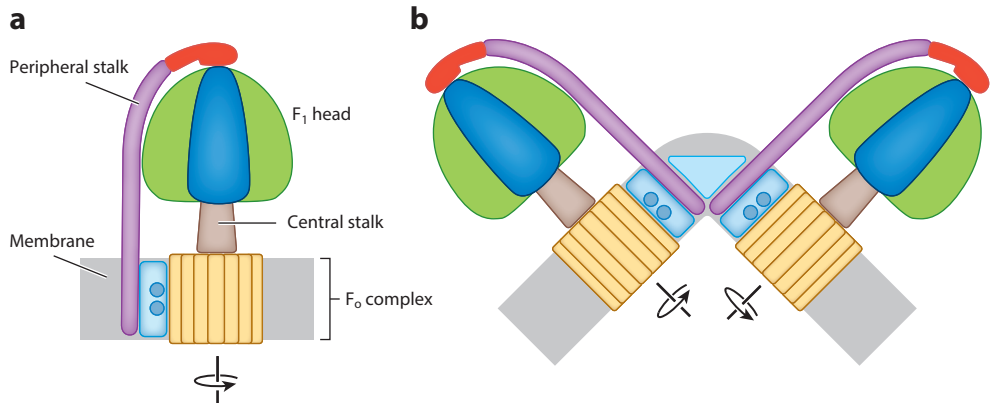

Figure 1

Schematic overview of F-type ATP synthases. F-type ATPases consist of a catalytic F_1 head and the F_o motor complex in the membrane. The F_1 head comprises three α-subunits and three catalytic β-subunits (*dark blue* and *green*) that generate ATP from adenosine diphosphate (ADP) and phosphate by rotary catalysis. The F_o motor consists of the *c*-ring rotor (*yellow*) and the *a*-subunit stator (*light blue*) with its conserved hairpins of membrane-intrinsic helices (*blue circles*). F_1 and F_o are connected by the central stalk (*brown*) and the peripheral stalk (*purple*). The peripheral stalk attaches to F_1 via a subunit known as δ in chloroplasts and bacteria or *OSCP* in mitochondria (*red*). In ATP synthesis mode, the *c*-ring rotates in counterclockwise direction (as seen from F_1) relative to the F_1 head, as indicated. In mitochondrial ATP synthase dimers, the two monomers operate independently. (*a*) Bacterial and chloroplast ATP synthases are monomeric. (*b*) Mitochondrial ATP synthases are dimers, linked in the membrane by an additional set of dimer-specific subunits (*light blue triangle*).

some make use of a sodium gradient instead (32). Ion selectivity depends on the exact, genetically programmed geometry of the ion-coordinating side chains in the *c*-ring subunit rotor (33).

Bacterial F-type ATPases are fascinating in their own right, and they have been invaluable for mutant studies, because neither mitochondria nor chloroplasts lend themselves easily to genetic manipulation. Most of the functionally important residues of F-type ATPases have been identified and investigated with *Escherichia coli* mutants (34–41). Moreover, bacterial F-type ATPases serve as important model systems for studying the universal rotary mechanism by single-molecule biophysics (42, 43). High-speed imaging of fluorescently labeled F_1 heads indicated that subunit γ rotates at a rate of 130 s^{-1} or higher, indicating that bacterial ATPases can hydrolyze or synthesize more than 400 molecules of ATP per second (44, 45).

The 6.9-Å cryo-EM structure of intact *E. coli* ATP synthase (46) resolved all α-helices in the complex (**Figure 2*a***). β-strands or amino acid side chains were not visible, as this would require a resolution of 4.5 Å or better. An atomic model was built on the basis of known high-resolution X-ray structures of conserved subunits and sequence homology. Image processing sorted particles into three rotational states, with the central rotor stalled in different positions related by ~120° steps. Subunit δ on top of the F_1 head was seen to bind to the three α-subunits. The peripheral stalk consisted of two identical *b*-subunits—long, single α-helices entwined in a loose coil. In the membrane, the *b*-subunit dimer bifurcated, clamping the F_o subunit *a* to the *c*-ring. At the opposite end, the two *b* helices again interacted differently with subunit δ that connects them to F_1. It is highly unusual to have two different, promiscuous interactions of the same conserved subunit in one protein complex.

The recent 2.9-Å cryo-EM structure of a bacterial ATP synthase from *Bacillus* PS3 expressed in *E. coli* (47) likewise shows three rotational states and confirms the path of proton translocation in the high-resolution cryo-EM structure of the related chloroplast ATP synthase (48), discussed in detail below.

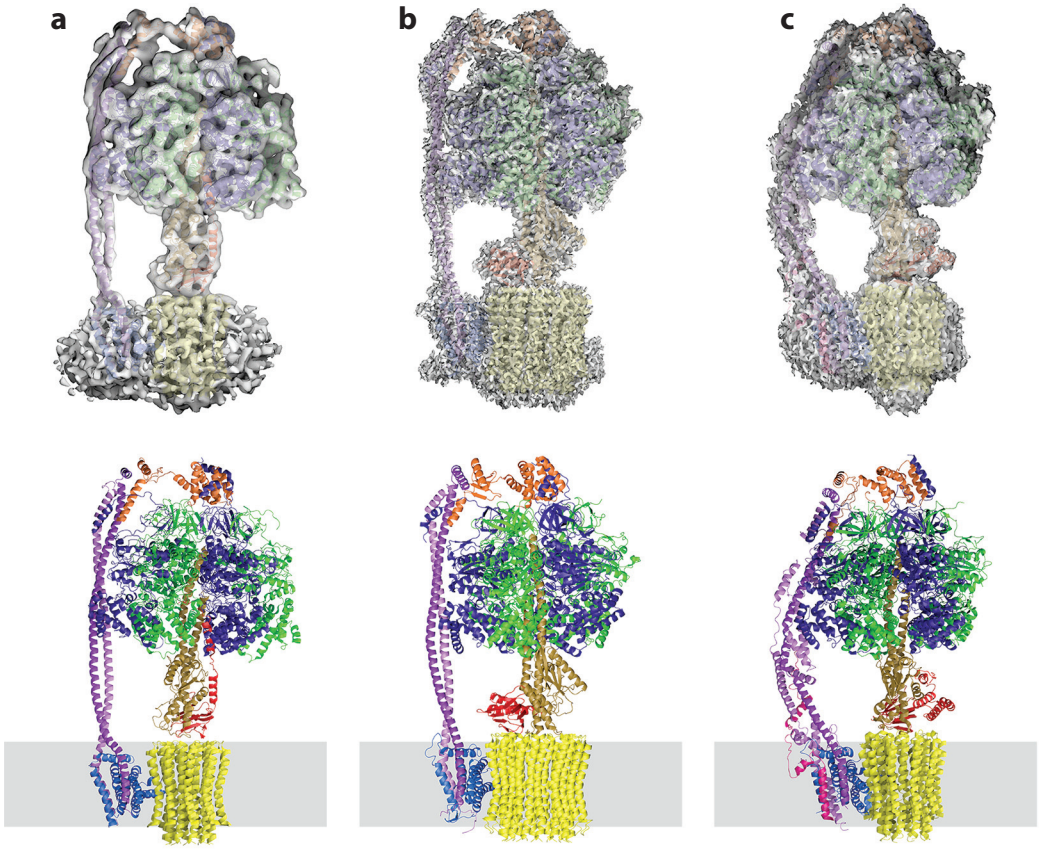

Figure 2

Cryo-EM maps and atomic models of three intact F-type ATP synthases. (*a*) Bacterial F-type ATPase. (*b*) Chloroplast ATP synthase (cF_1F_o). (*c*) One-half of a mitochondrial ATP synthase (mtF_1F_o) dimer. (*a*) The map resolution of the *Escherichia coli* complex is 6.9 Å (46). (*b*) The resolution of the Spinach chloroplast ATP synthase is 2.9 Å for F_1 and 3.4 Å for F_o (48). (*c*) The resolution of the ATP synthase monomer from *Saccharomyces cerevisiae* mitochondria is 3.6 Å (76). Subunit color codes: α (*dark blue*); β (*green*); δ (*orange*, in *E. coli* and chloroplasts); *OSCP* (*orange*, in mitochondria); *b* (*dark purple*); *b′* (*light purple*); *a* (*light blue*); *c*-ring (*yellow*); γ (*brown*); ε (*red*, in *E. coli* and chloroplasts) or δ and ε (*red*, in mitochondria). The five different peripheral stalk subunits in panel *c* are drawn in shades of purple.

The *E. coli* complex used for cryo-EM was autoinhibited by the central stalk subunit ε. The 3.3-Å X-ray structure of an *E. coli* $\alpha_3\beta_3\gamma\varepsilon$ complex (49) had shown that the C-terminal helix of ε swings up into the space between the central stalk and the α-/β-subunits, where it contacts γ and the C-terminal region of β, blocking rotation.

The 4-Å structure of the ATP synthase from *Paracoccus denitrificans* (50), a bacterial model for oxidative phosphorylation, is the only X-ray structure of an ATP synthase that contains all functionally relevant subunits. Like the *E. coli* structure, it is in an inhibited state, although in this case inhibition is effected by the regulatory ζ-protein of α-proteobacteria. Surprisingly, the F_o complex and peripheral stalk of the *P. denitrificans* structure were less complete and well resolved than in the 6.9-Å cryo-EM structure of the *E. coli* complex (46), perhaps owing to co-crystallization of different rotary states, which would impair crystal quality.

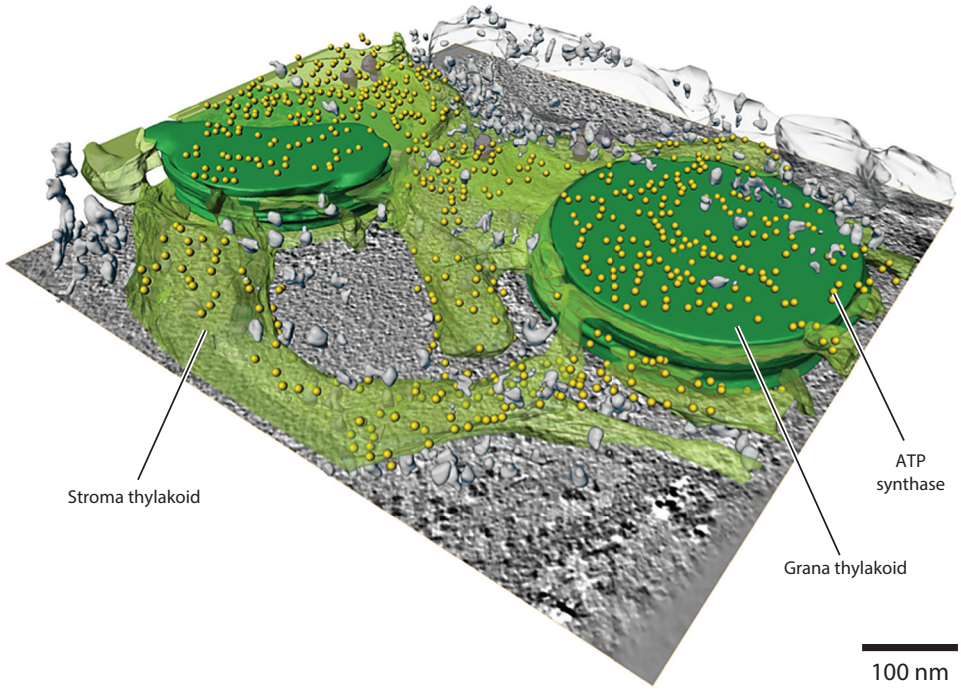

Figure 3

Cryo-ET of chloroplast thylakoid membranes. F_1 heads (*yellow*) of the chloroplast F_1F_o ATP synthase (cF_1F_o) are confined to stroma and grana end membranes. cF_1F_o is monomeric and not found at the highly curved grana edges. Grana stacks (*dark green*); stroma membranes (*transparent green*). Figure courtesy of Bertram Daum, Max Planck Institute of Biophysics.

CHLOROPLAST ATP SYNTHASE

Along with the cyanobacteria from which they originate, green plant chloroplasts have the extraordinary ability to capture and convert solar energy. ATP generated by photosynthesis is the prime source of biologically useful energy on Earth and a precondition for the development of other eukaryotic life forms. The chloroplast F_1F_o ATP synthase (cF_1F_o) is driven by the electrochemical proton gradient across the thylakoid membrane. The gradient is created by the water-splitting reaction of photosystem II and by light-driven, cyclic electron flow around photosystem I and the b_6f complex.

The chloroplast ATP synthase resembles the bacterial complex in size and subunit composition (**Table 2**). First insights into the cF_1F_o structure came from electron microscopy of negatively stained specimens (51), followed by an early cryo-EM study (52). Cryo-ET of chloroplast thylakoid membranes demonstrated that cF_1F_o is confined to grana end membranes and stroma thylakoids but not found on the highly curved grana edges (53, 54) (**Figure 3**). In contrast to mitochondrial ATP synthases, cF_1F_o is randomly distributed and monomeric in the thylakoid membrane (53). The monomeric state of cF_1F_o is not surprising, given that it lacks the dimer-specific subunits of the mitochondrial complex (**Table 2**). The same applies to bacterial ATP synthases, which can therefore all be assumed to be monomers as well.

The cryo-EM map of the complete, functionally competent cF_1F_o complex (48) achieved a resolution of 2.9 Å for the cF_1 head and 3.4 Å for the cF_o complex in the membrane (**Figure 2*b***). ADP molecules were resolved in the β_{DP} and β_{TP} sites. No inhibitors or ATP analogs had been

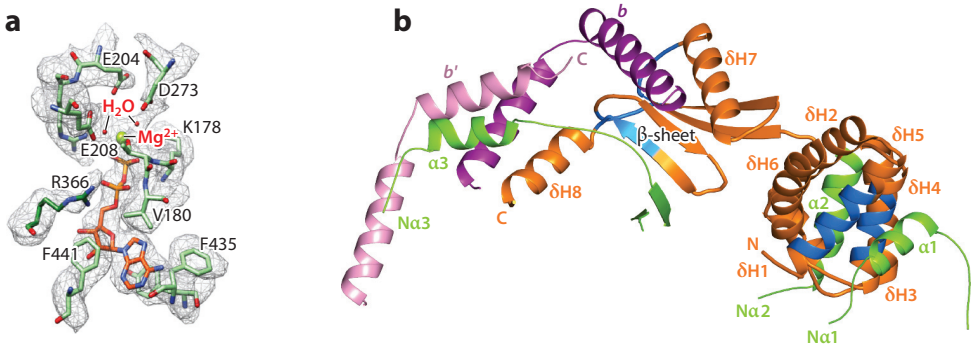

Figure 4

Details of chloroplast ATP synthase F_1 structure. (*a*) β_{TP} site in catalytic F_1 head. Adenosine diphosphate (ADP; *orange*), Mg^{2+} (*bright green*), water molecules (*red spheres*), and coordinating side chains (*stick representation*) in cryo-EM map density (*gray mesh*). Arginine 366 (R366; the so-called arginine finger) is contributed by subunit α. All other residues in the binding site belong to subunit β. ATP in this site hydrolyzed spontaneously to ADP during isolation (48). (*b*) Interactions of subunit δ on top of F_1 with α-subunits and peripheral stalk. Subunit color codes: δ (*orange*); N-terminal helices of α-subunits 1, 2, and 3 (*green*); *b* (*dark purple*); *b′* (*pink*); residues conserved in chloroplast δ and mitochondrial *OSCP* (*blue*).

added, and the β_E site was empty, as expected. ATP in the β_{TP} site had been hydrolyzed to ADP during isolation. The map showed not only the bound nucleotides but also the coordinating Mg^{2+} ions and water molecules (**Figure 4*a***). Water molecules would not be visible in an X-ray structure of the same nominal resolution. Structural details in cryo-EM maps are clearer owing to the high quality of structure factor phases recorded in the electron micrographs.

Subunit δ on top of the cF_1 head links the three α-subunits to the long peripheral stalk helices *b* and *b′*. The chloroplast δ-subunit consists of an N-terminal α-helical domain and a C-terminal domain containing a central β-sheet (**Figure 4*b***). The two domains are joined by a single polypeptide strand. The α-helical domain interacts closely with the N-terminal helices of two α-subunits, whereas the N terminus of the third α-subunit forms a helix bundle with the C-terminal helix of *b′*, the two C-terminal helices of *b* and a helix in the C-terminal domain of subunit δ. As in *E. coli*, the long, loosely entwined α-helices of the peripheral stalk bifurcate as they enter the lipid bilayer to clamp subunit *a* against the *c*-ring rotor (**Figure 2*b***). Subunit γ works as a redox-controlled regulator switching ATPase activity off at night; subunit *a* defines the proton access and release channels in F_o. Both are discussed in more detail below.

MITOCHONDRIAL ATP SYNTHASES

Mitochondrial ATP synthases (mtF_1F_o) not only differ from their bacterial and chloroplast counterparts but also vary greatly among themselves in terms of subunit composition (**Table 2**), structure, and membrane arrangement.

Mitochondrial ATP Synthase Dimers

The most striking feature of mitochondrial ATP synthases compared with other rotary ATPases, including V- and A-type, is that they all form dimers in the membrane (**Figure 5*a–d***), even though, in independent lineages, the dimerization interface is made up of different subunits with no apparent homology. The dimers assemble into long rows (**Supplemental Video 1**) or short ribbons at the cristae rims (**Figure 5*e–b***). The various forms of ATP synthase dimers result from

Supplemental Material >

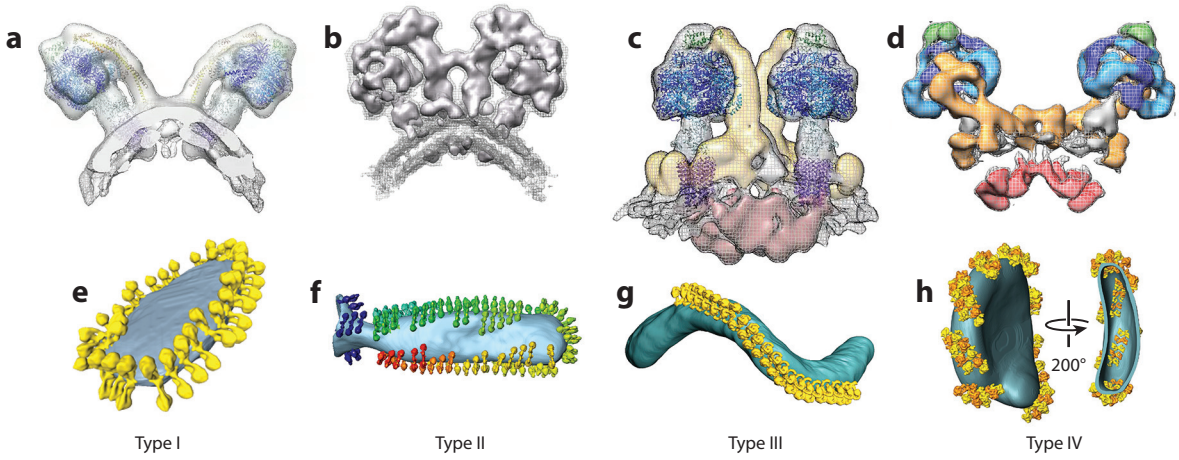

Figure 5

Cryo-ET of mitochondrial ATP synthase dimers. (*a–d*) Subtomogram averages and (*e–h*) 3D volumes of cristae vesicles are shown as follows: (*a,e*) *Saccharomyces cerevisiae*, (*b,f*) *Polytomella* sp., (*c,g*) *Paramecium tetraurelia*, and (*d,h*) *Euglena gracilis*. Subunits α, β, and δ in the F_1 head are drawn in shades of blue and green, and modeled *c*-ring rotors in panel *c* are purple. Peripheral stalk densities in panels *c* and *d* are light brown. Tones of red in panels *c* and *d* indicate bulky lumenal densities. Dimer rows in panels *e* and *g* are yellow. Short dimer ribbons in panel *f* are rainbow colored. In panel *h*, alternating interdigitated dimers (*yellow* and *orange*) form short ribbons at the ridges of disk-like cristae. The membrane is light blue. Panels *a* and *e* adapted from Reference 61, with the subtomogram average courtesy of Karen Davies, Max Planck Institute of Biophysics; panels *b* and *f* adapted from Reference 68; panels *c* and *g* adapted from Reference 71; and panels *d* and *h* adapted from Reference 72.

different contacts mediated by their peripheral stalks and F_o subunits. ATP synthase dimers were discovered by Blue Native polyacrylamide gel electrophoresis of mitochondrial membrane protein complexes (55). Electron microscopy of negatively stained complexes extracted from the gels (56) or of dimers prepared by density gradient centrifugation (57, 58) indicated that they comprise two F_1F_o monomers joined in a V shape.

So far, four different types of mtF_1F_o dimers, referred to as Types I–IV, have been characterized by cryo-ET. Major differences exist between ATP synthase dimers of various unicellular organisms (**Figure 5*a–d***). As only a few of their mitochondrial protein complexes have been explored in detail, more types of mtF_1F_o dimers are likely to emerge in future.

Type I dimers: animals and fungi. The best-known type of ATP synthase dimer with an angle of ~86° between its two central stalks is found in mitochondria from bovine heart (59), yeasts (60, 61), and fungi (62). Type I may include mitochondrial ATP synthases of vascular plants, although their dimer angles vary (60). Type I dimers associate loosely into long rows that engender high local membrane curvature at the edges of lamellar cristae (59, 61) (**Figure 5*e***; **Supplemental Video 1**). Subtomogram averages of *Saccharomyces cerevisiae* dimers imaged in situ (61) resolved the central and peripheral stalks as well as the catalytic subunits in the F_1 head (**Figure 5*a***). Mammalian and yeast mtF_1F_o dimers are indistinguishable at low resolution (60), and their subunit composition is similar (**Table 2**).

Supplemental Material >

Type II dimers: unicellular green algae. Another well-characterized type of mitochondrial ATP synthase dimer is that of the unicellular, chlorophyll-less green alga *Polytomella* sp. (63) and its close relatives, including the photosynthetic model organism *Chlamydomonas reinhardtii*. *Polytomella* mtF_1F_o has been investigated by proteomics (64), protein sequencing (65), chemical cross-linking (66), negative-stain electron microscopy (57), and cryo-ET (67, 68). The F_1 head, central

stalk, and *c*-ring rotor resemble those of other ATP synthases (**Table 2**), but in addition, Type II has a set of unique ATP synthase-associated (*ASA*) subunits (69). The *ASA* subunits form the massive peripheral stalk that is the hallmark of Type II dimers (**Figure 5*b***). The angle between the central stalks is 56°. The larger size and apparent solidity of the *Polytomella* dimer make it an attractive target for high-resolution studies by single-particle cryo-EM.

Type III dimers: ciliates. Rows of dimeric particles thought to be ATP synthases were observed in deep-etched tubular cristae of the ciliate *Paramecium multimicronucleatum* (70). Proof of their identity came from cryo-ET and subtomogram averaging (71). The subtomogram average of *Paramecium* dimers (71) resolved the α-/β-subunits in the F_1 head and the central and peripheral stalks (**Figure 5*c***). The dimers are U shaped rather than V shaped, the dimer angle is close to zero, and the peripheral stalks are laterally offset. Large lumenal protein densities mediate close interdimer contacts that result in unusually long and regular helical rows (71) (**Figure 5*g***).

Type IV dimers: *Euglena* and trypanosomes. Mitochondrial ATP synthase dimers of the ciliated green alga *Euglena gracilis* and the related sleeping-sickness parasite *Trypanosoma brucei* share some characteristics with Type III (**Figure 5*d***). Their peripheral stalks are offset, and they have similar, although less bulky, lumenal densities (72). The Type IV F_1 head is pyramid shaped rather than globular (72), on account of its euglenozoa-specific subunit *p18* (73, 74). The Type IV dimer angle is ~55°. As in Type III, subunits of the peripheral stalk and lumenal densities remain to be explored.

Single-Particle Electron Cryo-Microscopy Structures of Mitochondrial ATP Synthases

Rapid progress has been made in determining the structures of mitochondrial ATP synthases by single-particle cryo-EM. In the past three years, a total of six structures have been obtained at increasing resolution, including the bovine mtF_1F_o monomer (75), mtF_1F_o monomers from two yeasts (76, 77), the F_o dimer of *S. cerevisiae* without F_1 heads or stalks (78), and two complete dimers of Types I (79) and II (80, 81) (**Table 1**).

Structures of yeast ATP synthase. The ATP synthase of the obligate aerobic yeast *Yarrowia lipolytica* resembles that of baker's yeast (*S. cerevisiae*) closely. The dimer-specific subunits of yeast and bovine mtF_1F_o are also similar (**Table 2**). Mammalian mtF_1F_o dimers are potentially relevant to human health, but they are less stable than those of yeast and therefore less tractable. Their relative stability and resemblance to mammalian dimers make yeast dimers interesting for structural studies. Crystallization trials with purified *Y. lipolytica* dimers produced crystals of a core complex consisting of the F_1 head, central stalk, and c_{10} rotor ring (79), as had been the case with mtF_1F_o from *S. cerevisiae* (25). Single-particle cryo-EM of the *Y. lipolytica* complex yielded a 6.2-Å map (**Figure 6*a***) as the first structure of an intact Type I dimer (79). Activity measurements indicated that the two F_1F_o monomers in the dimer work independently of one another (79).

The yeast F_o complex contains up to six small hydrophobic subunits responsible for dimer formation and stability (61, 82) (**Table 2**). Eleven helix densities were resolved in the F_o region of the *Yarrowia* dimer and assigned to the membrane subunits of yeast F_o (79). The assignment was unambiguous for subunit *a*, on account of its long and highly tilted, membrane-intrinsic helices (83), but tentative for the others. The definition of the *Yarrowia* dimer map was limited, partly due to small variations in dimer angle and the superposition of different rotary states (79). To improve the resolution, three strategies seemed promising: (*a*) to cleave F_1 off and determine the structure of the F_o dimer separately; (*b*) to isolate the monomer and determine its structure instead;

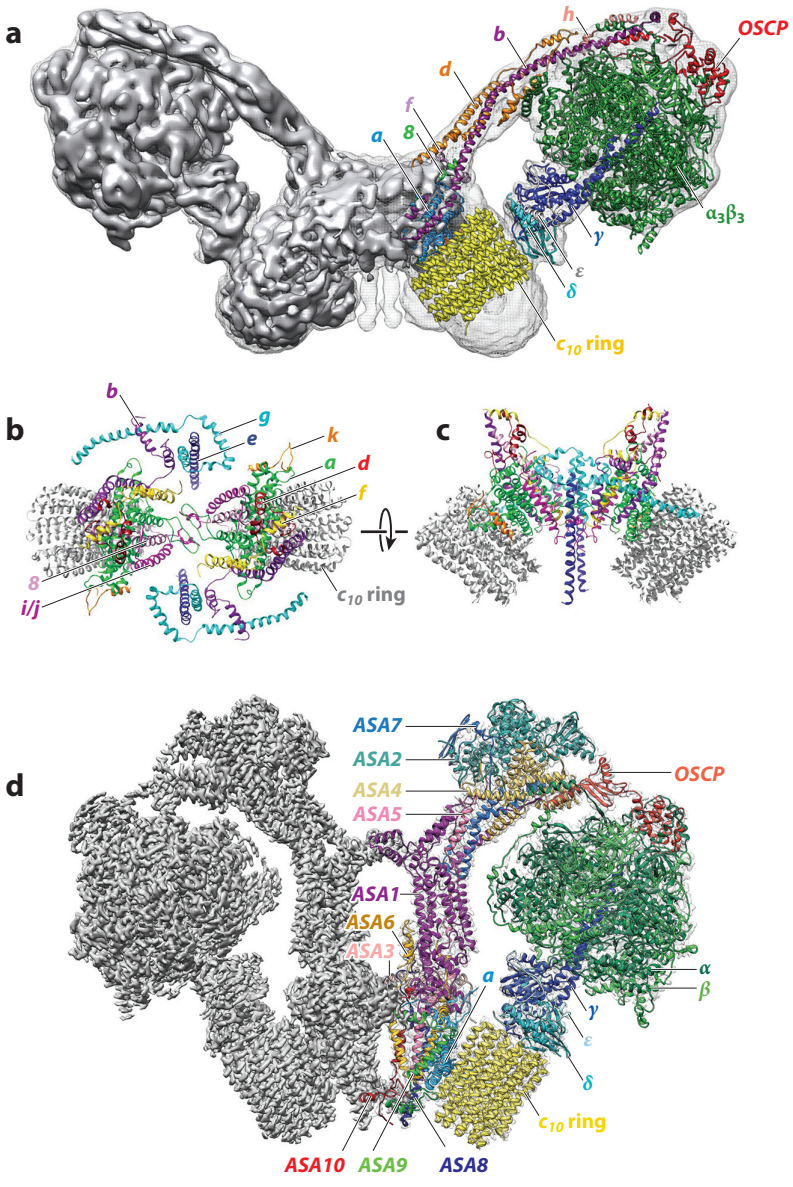

Figure 6

Single-particle cryo-EM structures of mitochondrial ATP synthase dimers with labeled subunits (see **Table 2**). (*a*) 6.2-Å map (*gray*) and model of the *Yarrowia lipolytica* F_1F_o dimer (79); (*b*,*c*) 3.6-Å model of the *Saccharomyces cerevisiae* F_o dimer (78); and (*d*) 2.7-Å map (*gray*) and atomic model of the F_1F_o dimer from *Polytomella* sp. (81). All structures drawn to the same scale. Panel *a* adapted from Reference 79. Panels *b* and *c* adapted from Reference 78. Panel *d* courtesy of Bonnie Murphy and Niklas Klusch, Max Planck Institute of Biophysics.

or (*c*) to choose a more rigid dimer. All three strategies were pursued independently by three groups, and all resulted in higher-resolution structures (76, 78, 81). The 3.6-Å structure of the *S. cerevisiae* F_o dimer without F_1 heads (78) (**Figure 6*b,c***) presented an unambiguous atomic model of subunits *a*, *b*, *d/F6*, *e*, *f*, *g*, *i/j*, *k*, and *8* (**Figure 2*c***) and confirmed the subunit *a* assignment in *Yarrowia*.

The structure of the *S. cerevisiae* monomer was determined with and without oligomycin (76). Four copies of the inhibitor were found to bind to the *c*-ring in the same conformation as in the X-ray structure of isolated *S. cerevisiae c*-rings (84). The bulky inhibitor impedes ring rotation and blocks mitochondrial ATP synthase in both directions.

Structure of the *Polytomella* Type II dimer. *Polytomella* mitochondria contain the largest-known ATP synthase. Its two massive peripheral stalks are joined by a protein bridge ~65 Å above the membrane surface, enhancing the stability of the 1.6-MDa dimer. Single-particle analysis yielded a structure at 6.2 Å (83), then at an overall resolution of 4.1 Å (80), which has since been improved to 2.7 Å (81) (**Figure 6*d***; **Supplemental Video 2**). An atomic model of the 2,500 residues in the peripheral stalk subunits was built de novo. In combination with mass spectrometry and genome sequencing, ten different *ASA* subunits were identified and fitted, including one that was previously unknown (81). The contact between subunit *a* and the membrane-spanning subunit *ASA6* that contributes to forming the proton access channel is mediated by a lipid molecule (80). The critical subunit *a* that forms the proton access and release channels is discussed in more detail below.

Supplemental Material >

INSIGHTS FROM THE NEW STRUCTURES OF COMPLETE ATP SYNTHASES

The cryo-EM structures of F-type ATP synthases have produced a wealth of unexpected new insights into the roles of the central and peripheral stalks, the structures and populations of different rotary states and substates, the structure and dynamic role of the *δ/OSCP* subunit, the detailed structure of subunit *a* and its aqueous membrane channels, the generation of torque in F_o and how it drives the rotation of differently sized *c*-rings, redox regulation in plants, the mechanics of dimer formation, and how mitochondrial ATP synthase dimers shape the cristae.

Rotary States and Substates

Synthesis or hydrolysis of ATP by rotary catalysis proceeds in three ~120° steps, sometimes referred to as power strokes (85), that add up to a full 360° turn of F_o against the F_1 head (**Supplemental Videos 2** and **3**). Each step is associated with a rotary state, in which the rotor assumes discrete positions relative to F_1. Image processing of the *E. coli* (46), bovine heart (75), *Polytomella* (81), and chloroplast ATP synthase (48) resolved three primary rotary states with the central rotor in different positions (**Figure 7*a–c***). Each of the primary rotary states represents a distinct stage of the catalytic cycle. In the mitochondrial ATP synthases from bovine heart and *Polytomella*, the three primary rotary states were resolved into a total of 7 (75) and 13 (81) transient substates. In the autoinhibited chloroplast complex (48), the primary rotary states were not separated by exactly 120° nor did the rotary angles correspond to the nearest integral number of *c*-ring subunits predicted from the symmetry mismatch between the 14-fold rotor and the 3-fold F_1 head, which would be 103°, 129°, and 129°, corresponding to 4, 5, and 5 *c*-ring subunits. Instead, the rotary states were separated by unequal steps of 103°, 112°, and 145° (**Figure 7*f***), corresponding to 4, 4.4, and 5.6 *c*-ring subunits (48) (**Figure 7*g***). Because each *c*-ring subunit translocates one proton per 360° turn of the *c*-ring, and given that the free energy ΔG of ATP hydrolysis is close to −50 kJ/mol (86), the energy contributions due to proton movement for progressing from one state to the next are

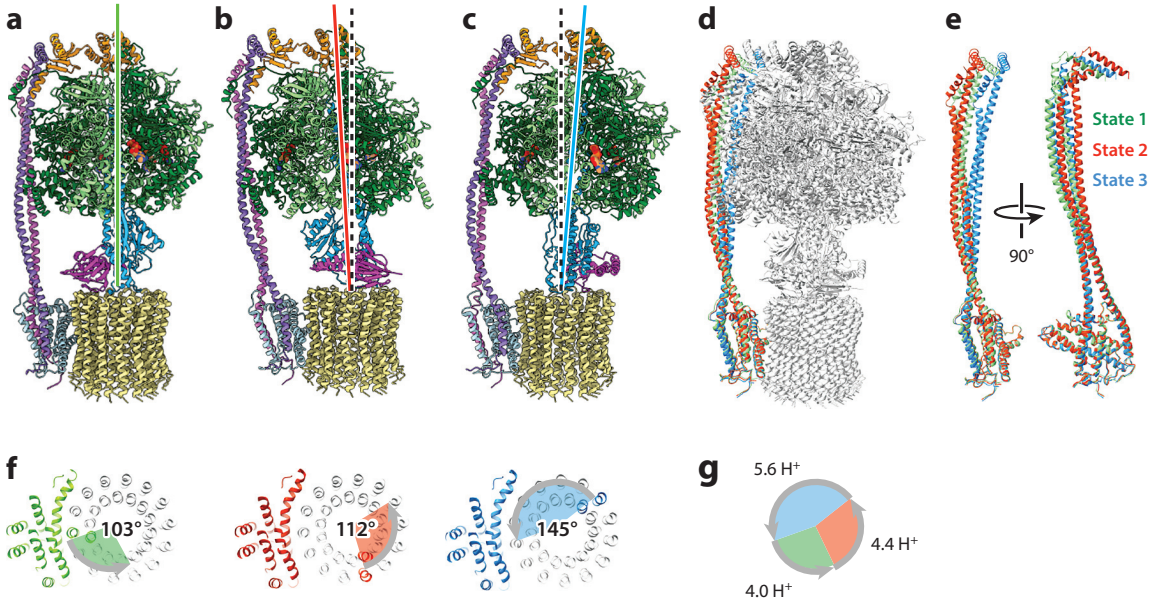

Figure 7

Three rotary states of chloroplast ATP synthase. Image processing revealed three different rotary states with different particle populations. (*a*) State 1 was the most populated (85% of particles), indicating it is the most stable. (*b*,*c*) In states 2 and 3, the F_1 head and γ-subunit are tilted by 5° and 11.5° relative to state 1 (*red* and *blue lines*), resulting in precession of F_1 around the central axis (*dashed black line*) during rotary catalysis. (*d*) Superposition of the three rotary states, with peripheral stalk and subunit *a* in color. (*e*) Two orthogonal views of superposed peripheral stalks indicating flexibility. (*f*) Rotation angles of *c*-ring rotor relative to subunit *a*. (*g*) Number of translocated protons required to progress from one state to the next. Figure adapted from Reference 48.

−43.7, −48.1, and −61.2 kJ/mol. The three primary rotary states represent local energy minima or resting positions in the catalytic cycle that must result from subunit interactions in the whole complex. The three resting positions of high, medium, and low probability observed by single-molecule light microscopy of *E. coli* F_1F_o (87) are consistent with the three primary rotary states of cF_1F_o that are populated by 85%, 8%, and 7% of the particles, as indicated by cryo-EM (48).

The Central Stalk

The central stalk transmits torsional force from the F_o motor to the catalytic sites in the F_1 head and is an indispensable part of all ATP synthases. Subunit γ, its principal component, is firmly but reversibly attached to the *c*-ring rotor by a number of salt bridges. The central stalk of mitochondrial ATP synthases contains two smaller subunits termed δ and ε that reinforce interaction with the *c*-ring rotor. The mitochondrial subunits δ and ε have derived their names by historical accident (see section titled The Need for a Unified ATP Synthase Nomenclature below) and are unrelated to the eponymous subunits of bacteria and chloroplasts. The central stalk subunit ε autoinhibits some bacterial ATP synthases (46, 49). In chloroplasts, autoinhibition is effected by a pair of β-hairpins in the γ-subunit that blocks rotation when the redox potential becomes oxidizing, as discussed in more detail below.

Single-molecule experiments (42, 85, 87) and computer simulations (88) have been taken to suggest that the central stalk subunit γ serves as an elastic buffer of torsional energy during rotation. However, the 3 rotary states in the cryo-EM structures of chloroplast (**Figure 7**) and *E. coli* (46) ATP synthase, the 7 rotary substates of the bovine monomer (75), and the 13 rotary

substates of *Polytomella* ATP synthase (81) all show subunit γ in essentially the same conformation, indicating that it moves as a rigid body. Comparative analysis of the rotary states and substates of the high-resolution *Polytomella* ATP synthase structure (81) suggests that the whole F_1 head rotates along with the central stalk and *c*-ring rotor for the first 20–30° of a power stroke, equivalent to approximately one *c* subunit, and then recoils to the starting position of the next power stroke (**Supplemental Video 3**). The 7 substates of the bovine monomer (75), albeit at 7-Å resolution, are consistent with this new and unexpected modification of the well-established rotary mechanism. The concerted movement of F_1 and γ ensures flexible coupling of the symmetry-mismatched F_1 and F_o subcomplexes, as required for rotary catalysis, and obviates the need for an elastic central stalk. Single-molecule measurements with *E. coli* F_1F_o indicate rotary substeps that can push rotation back by as much as one *c*-ring subunit during a power stroke (87). The concerted rotation of F_1 and central stalk for part of an ~120° step thus appears to be common to the rotary mechanism of all F-type ATP synthases.

Supplemental Material >

The Peripheral Stalk

Bacterial and chloroplast ATP synthases have thin, slender peripheral stalks (**Figure 2*a,b***) that consist of no more than two long, loosely entwined α-helices of subunits *b* and *b′* (which are identical in many bacteria, including *E. coli*). They are anchored by one membrane-spanning helix each and extend 110 Å to the *δ*-subunit at the top of F_1.

Cryo-EM structures of the three main rotary states in the intact chloroplast ATP synthase (48) reveal that the peripheral stalk flexes by up to 12° during rotation (**Figure 7*d,e***) and therefore can store elastic energy. The three rotary states of *E. coli* (46) indicate similar degrees of peripheral stalk flexibility. In the monomeric bacterial and chloroplast ATP synthases, the peripheral stalk appears to act as an elastic spring that evens out energy minima between rotary states and thus contributes to the flexible coupling of F_1 to F_o.

Peripheral stalks of yeast (76) and bovine mitochondrial ATP synthase (75) are more substantial. They all have one long unbroken helix (subunit *b*) plus another five α-helical subunits termed *8*, *F6*, *d*, *f*, and *i* or *j* in yeast (**Table 2**) (**Figure 2*c***); subunit *8* is an evolutionary remnant of the bacterial peripheral stalk helix *b′* (79). Together, the peripheral stalk subunits of yeast and mammalian ATP synthases form a discontinuous helix bundle that is anchored in the membrane by the single-span hydrophobic helices of subunits *b*, *d*, *f*, and *i/j*. The massive peripheral stalk of *Polytomella* ATP synthase flexes only minimally during rotary catalysis (81).

In terms of subunit composition, sequence, and structure, the bulky peripheral stalks of Type II mitochondrial dimers (including *Polytomella*) are unrelated to those of bacterial and chloroplast monomers or of Type I dimers. They are linked on the matrix side by interacting helix hairpins above the membrane (**Figures 5*b*** and **6*d***), which would constrain their movement. The subunit composition and detailed structure of Type III and IV peripheral stalks are unexplored.

Subunits *δ* and *OSCP*

The subunit connecting the F_1 head to the peripheral stalk is known as *δ* in chloroplasts and bacteria but *OSCP* in mitochondria. It consists of an N-terminal α-helical domain connected by a short stretch of polypeptide to a C-terminal domain containing a central β-sheet. The structure of the N-terminal domain had been determined by NMR (89, 90), whereas that of the C-terminal domain was unknown. In the high-resolution cryo-EM structures of cF_1F_o (48) (**Figure 4*b***) and of *Polytomella* ATP synthase (81), *δ* and *OSCP* look alike. Sequence comparison of bovine *OSCP* and Spinach chloroplast *δ* indicates that 23% of their residues are identical and 49% are conserved,

confirming that δ and *OSCP* are essentially the same protein. These findings mean that the structure and function of *δ/OSCP* have remained unchanged over an evolutionary distance of 1.5 billion years (91, 92), or possibly longer. The most highly conserved regions are those that interact with the C-terminal helix of the peripheral stalk subunit *b* in cF_1F_o, or with the N-terminal helices of the three F_1 α-subunits (**Figure 4*b***). Remarkably, these three interactions are all different, even though the α-subunit sequences are identical.

In all previous models of F-type ATP synthases, the *δ/OSCP* subunit was assumed to form a rigid link between the peripheral stalk and the F_1 head. The 13 different rotary states and substates of the *Polytomella* ATP synthase (81) indicate, however, that *δ/OSCP* acts as a hinge. The N-terminal domain that connects to the three α-subunits pivots against the C-terminal domain by 20 to 30° at the flexible single-polypeptide stretch connecting the two domains (**Supplemental Video 4**). The hinge movement enables the joint rotation of the F_1 head and central stalk for the first 20–30° of the ~120° power stroke.

Supplemental Material >

It is interesting to note that the C-terminal domain of *δ/OSCP* resembles the C-terminal domain of peripheral stalk subunit *E* in the A-type ATPases (48). A-type ATPases have two separate peripheral stalks that each bind to the F_1 head via their C-terminal domains (93). The central position of the N-terminal domain on F_1, plus the fact that it has only one such C-terminal domain, ensures that only one peripheral stalk can bind to F_1 in the F-type ATPases.

The Need for a Unified ATP Synthase Nomenclature

As exemplified by subunits δ, *OSCP*, and ε, the ATP synthase nomenclature can be perplexing, because it evolved from different nomenclatures for bacteria, chloroplasts, and mitochondria. Each was originally based on the order of bands on a gel, often without knowledge of the exact location or role of the corresponding subunit in the complex. This explains the different names of *OSCP* and δ for a component that performs the same role in all F-type ATP synthases. However, the confusion does not end there. In mitochondria, δ refers to a subunit of the central stalk that is homologous to bacterial ε but bears no resemblance to *OSCP* or the chloroplast and bacterial δ. To make matters worse, the central stalk of mitochondrial Type I ATP synthases contains another small subunit termed ε, although it is not related to the bacterial ε (see **Table 2**). The medical literature uses yet another nomenclature for human ATP synthase, whereby F_o subunits *a* and *8*, which carry many disease-relevant mutations, are variously referred to by their gene names as *ATP6* and *ATP8*, *MT-ATP6* and *MT-ATP8*, or sometimes, more correctly, by their gene product names as *Atp6p* and *Atp8p* (94). Subunits *j* (occasionally referred to as *i*) and *k* are known as *6.8PL* and *DAPIT*, respectively (95) (see **Table 2**). Now that the structures of complete bacterial, chloroplast, and mitochondrial ATP synthases have been determined, the time has come for a unified subunit nomenclature that applies to all. A new, consistent nomenclature of ATP synthase subunits will require the concerted action of research groups active in the field.

Regulation of ATPase Activity

Because they are fully reversible, ATP synthases need to be turned off when synthesis stops, to prevent uncontrolled ATP hydrolysis. Different regulatory mechanisms have evolved that engage different ATPase subunits or separate small proteins. Most of the currently known mechanisms work by blocking rotary hydrolysis through reversible interaction with subunit β in the F_1 head. Mammalian and yeast ATP synthases are regulated by the small inhibitory protein IF_1 (96–98). Active IF_1 is a dimer that forms under acidic conditions—for example, during ischemia, when the matrix pH can drop below 7 and glycolysis is the only source of cellular ATP. Monomeric

IF_1 is visible in the 6.2-Å map of the *Yarrowia* dimer, where it binds to an α_{DP}/β_{DP} site (79) at the negatively charged DELSEED motif near the C terminus of the β subunit, as in the X-ray structure of bovine F_1–IF_1 complex (99). The shape and dimensions of the IF_1 dimer suggest that it can bind to two F_1 heads simultaneously (100), but the two F_1 heads within one Type I dimer of yeast or mammalian ATP synthase are too far apart for this to happen in situ. However, the F_1 heads of two subsequent Type I dimers in a row are close enough for cross-linking by dimeric IF_1 (**Figure 5*e***), and this would be an excellent way of blocking ATPase activity.

In bacteria, the autoinhibitory ε-subunit of *E. coli* ATP synthase interacts with the DELSEED motif of the β_{DP} subunit (46, 101), as does IF_1 in mitochondria. The inhibitory ζ-subunit of α-proteobacteria resembles IF_1 and binds to the F_1 head in the same way (50).

Plants must shut off cF_1F_o at night to prevent unproductive ATP hydrolysis when the chloroplast redox potential does not sustain ATP synthesis. The chloroplast complex is regulated by a special redox mechanism (102) involving two β-hairpins of the γ-subunit that are arranged in an L shape (**Figure 8**). Under oxidizing conditions, two cysteine residues (103) in the shorter arm of the L form a disulfide bridge that stabilizes the β-hairpin of the longer arm, which binds to the DELSEED motif of the β_E subunit to block rotation and prevent ATP hydrolysis. Under reducing conditions, the disulfide bridge opens, the longer hairpin relaxes, and the γ-subunit can rotate freely.

Several modulators or inhibitors of F-type ATP synthases that affect cellular physiology, including the regulator of mitochondrial permeability transition, cyclophilin-D (104), act on *δ/OSCP*. These findings cannot be reconciled with the old model of *δ/OSCP* as a static connector, but they agree very well with the newly discovered role of *δ/OSCP* as a flexible hinge between F_1 and F_o (81).

Rotor Ring Size

A striking difference between the various F-type ATPases is the size of their *c*-ring rotors (**Figure 9**). The ring stoichiometry ranges from 8 *c*-ring subunits in mammalian mitochondria (75, 105) to 14 in chloroplasts (48, 106) and 15 in cyanobacteria (107, 108). The largest *c*-ring rotor discovered so far is that of the human pathogen *Burkholderia pseudomallei*, which has 17 subunits (109). There is no principal reason why larger rings should not exist. Indeed, the rotor ring of the A-type ATPase from *Enterococcus hirae* has 10 *K*-subunits, each with 2 helix hairpins (but only 1 proton binding site) (110), resulting in a ring size equivalent to 20 *c*-ring subunits. At the other end of the scale, the c_8 rotor of bovine mitochondrial ATP synthase is the smallest known. Rings with fewer than 8 *c*-ring subunits might not produce sufficient torque to deliver 3 molecules of ATP per turn, and F_o assemblies with such small rotors may not be stable.

Perhaps even more surprising than the variation of *c*-rings between species is their constant size within any one species. The stoichiometry of bacterial *c*-rings is species specific, is independent of growth conditions, and can be changed only by genetic engineering (111, 112). The ring size depends on the precise sequence and shape of side chains in the contact region between adjacent subunits (111), which is genetically programmed. The interaction motif is an xGxGxGxG repeat in the inner, N-terminal helix of the *c*-ring subunit hairpin (112), where G is a small hydrophobic residue (most often glycine but sometimes alanine) and x is a larger hydrophobic (valine, isoleucine, phenylalanine) or polar (asparagine) residue. The interaction motif ensures close packing of the inner helices against one another (113).

The number of *c*-ring subunits in the ring appears to be an adaptation to optimal growth conditions or to the physiological environment where the ATPases operate. For example, the c_{17} ring of *B. pseudomallei* ATPase would be an efficient proton pump to counteract the influx of

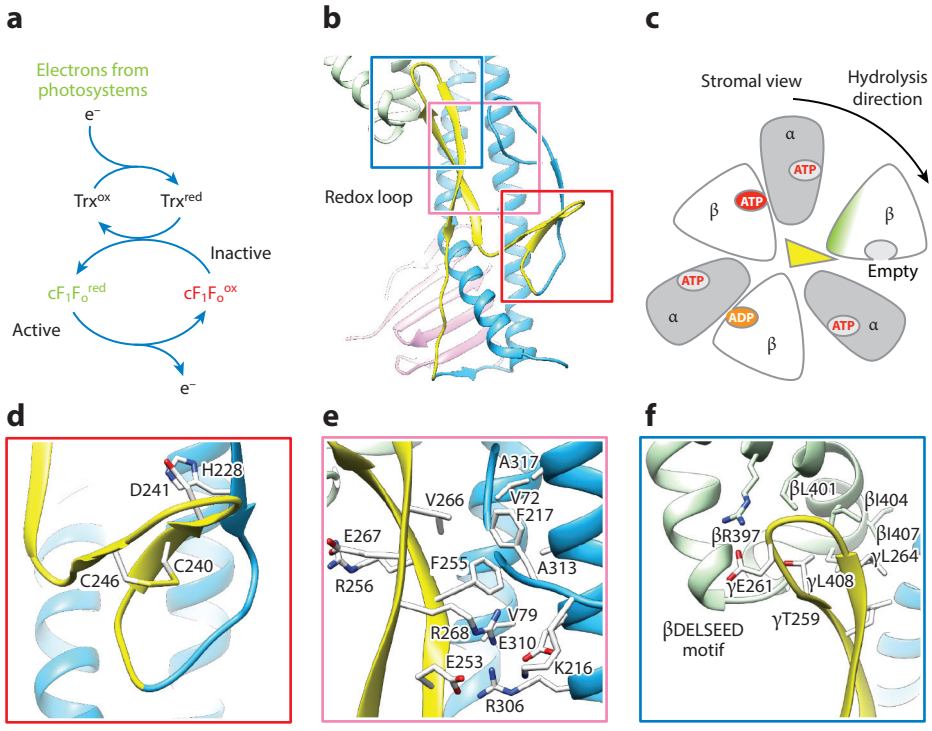

Figure 8

Redox regulation of chloroplast ATP synthase. (*a*) Electrons from photosynthesis reduce thioredoxin (Trx) in the chloroplast stroma, which converts oxidized, inactive cF_1F_o into the active, reduced form. The reverse process switches cF_1F_o off when Trx becomes oxidized, to prevent ATP hydrolysis at low light. (*b*) Subunit γ of cF_1F_o (*light blue*) contains a 40-residue L-shaped insertion of two β-hairpins (*yellow*) that inhibit cF_1F_o reversibly in response to the chloroplast redox potential. (*c*) The longer hairpin (*yellow triangle*) clashes with the C-terminal DELSEED motif of β_E (*green*) when the rotor turns in hydrolysis direction. (*d*) Two cysteines in the shorter arm of the L form a disulfide bond under oxidizing conditions, reinforcing the longer arm of the L in the space between γ and β_E. (*e*) The conserved γF255 interacts with γF217 in a hydrophobic pocket of the central stalk. (*f*) γE261 in the longer arm of the L forms a salt bridge with R397 of β_E, blocking rotation. Figure adapted from Reference 48; panels *a* and *c* drawn by Alexander Hahn, Max Planck Institute of Biophysics.

protons from the hostile acidic environment of the host cell phagosome (109). This type of ATPase is sometimes referred to as N-type (114). In addition to the N-type ATPase, *B. pseudomallei* and related bacteria have a regular F-type that is thought to have a smaller *c*-ring.

The *a*-Subunit

Subunit *a*, the largest of the hydrophobic F_o subunits, remained intractable and enigmatic for decades. Its main role is to conduct protons that drive rotary catalysis to and from the *c*-ring rotor. In the F_o motor assembly, subunit *a* functions as the stator that is held by the peripheral stalk against the *c*-ring rotor, forming a proton-tight dynamic seal. Attempts to express subunit *a* for crystallization as a stable, separate entity or as part of a complex invariably failed. In retrospect, this lack of success is hardly surprising, as the subunit harbors a cluster of charged and polar residues in four membrane-intrinsic, otherwise hydrophobic α-helices (**Figure 10**). Unpredictably, the

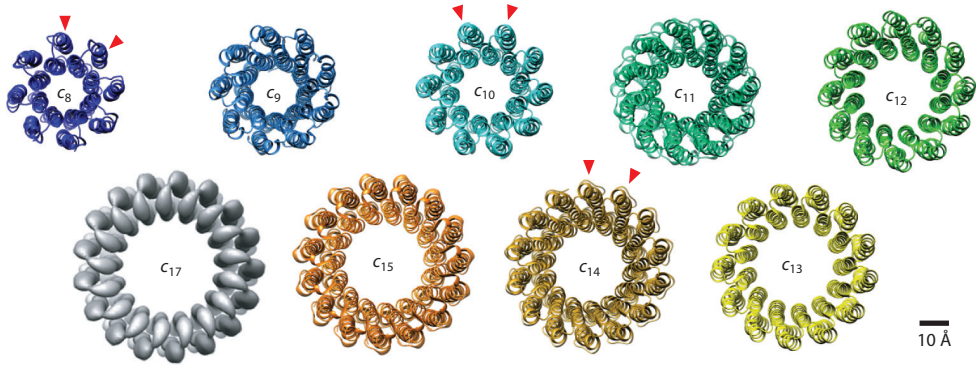

Figure 9

Structures of *c*-ring rotors. Top row from left: c_8 ring of bovine mitochondria (*dark blue*; PDB code 2XND) (105); c_9 ring of *Mycobacterium phlei* (*blue*, PDB code 4V1G) (146); c_{10} ring of *Saccharomyces cerevisiae* mitochondria (*light blue*, PDB code 3U2Y) (124); c_{11} ring of *Ilyobacter tartaricus* (*cyan*, PDB code 1YCE) (27); and c_{12} ring of a *Bacillus pseudofirmus* OF4 mutant (*green*, PDB code 3ZO6) (112). Bottom row from right: c_{13} ring of wildtype *B. pseudofirmus* OF4 (*yellow green*, PDB code 4CBJ) (152); c_{14} ring of *Pisum sativum* chloroplasts (*light brown*, PDB code 3V3C) (106); c_{15} ring of the cyanobacterium *Spirulina platensis* (*orange*, PDB code 2WIE) (108); and c_{17} ring of the human pathogen *Burkholderia pseudomallei* (*gray*, EMD code 3546) (109). The c_{17} ring is a 6-Å cryo-EM structure. All others are X-ray structures. Arrowheads indicate the positions of conserved protonation sites in adjacent *c*-ring subunits that are separated by a distance of ∼12 Å. All drawn as seen from F_1. Abbreviations: EMD, Electron Microscopy Data Bank; PDB, Protein Data Bank.

polar cluster is located in the hydrophobic core of the complex. Numerous mutagenesis and cross-linking studies (34–37) were taken to indicate that subunit *a* of *E. coli*, like most other membrane proteins known at the time, consisted of conventional transmembrane α-helices oriented more or less perpendicular to the membrane plane. This notion was supported by a 9.7-Å cryo-EM map of the *Thermus thermophilus* V-type ATPase (93). Subunit *I* of the V-type ATPase is the equivalent of the F-type subunit *a*, and the low-resolution map suggested a number of short helices that were proposed to form two transmembrane four-helix bundles, apparently consistent with the *E. coli* cross-linking results (34–37).

To some, it came as a shock when the 6.2-Å cryo-EM structure of the *Polytomella* ATP synthase (83) showed that the *a*-subunit helices were up to 80 Å long (more than twice the thickness of a lipid bilayer) and arranged in two hairpins that are almost entirely membrane embedded (**Figure 11**). The key feature of four long, near-horizontal *a*-subunit helices H3 to H6 in the membrane next to the *c*-ring has since been observed at increasing resolution in all recent cryo-EM structures of F-type ATPases (46, 48, 75, 76, 78–81) (**Table 1**). Higher-resolution structures of the *T. thermophilus* V-type ATPase motor assembly show two long *I*-subunit helices in the positions of H5 and H6 in subunit *a* (115, 116). A hairpin of two long, membrane-intrinsic helices at roughly right angles to the rotor ring is conserved in all rotary ATPases (117) and appears to be of ancient origin. H5, the longest of the *a*-subunit helices, has a characteristic stretch of conserved, charged, and polar side chains on either side of a strictly conserved arginine (**Figures 10** and **11**) that is essential for coupling proton translocation to ATP synthesis (38, 39, 118).

Proton Access and Release Channels

Atomic models of the *Polytomella* (80, 81) and chloroplast F_o complexes (48) were analyzed for aqueous cavities (119). Both structures indicated essentially the same proton access channel from

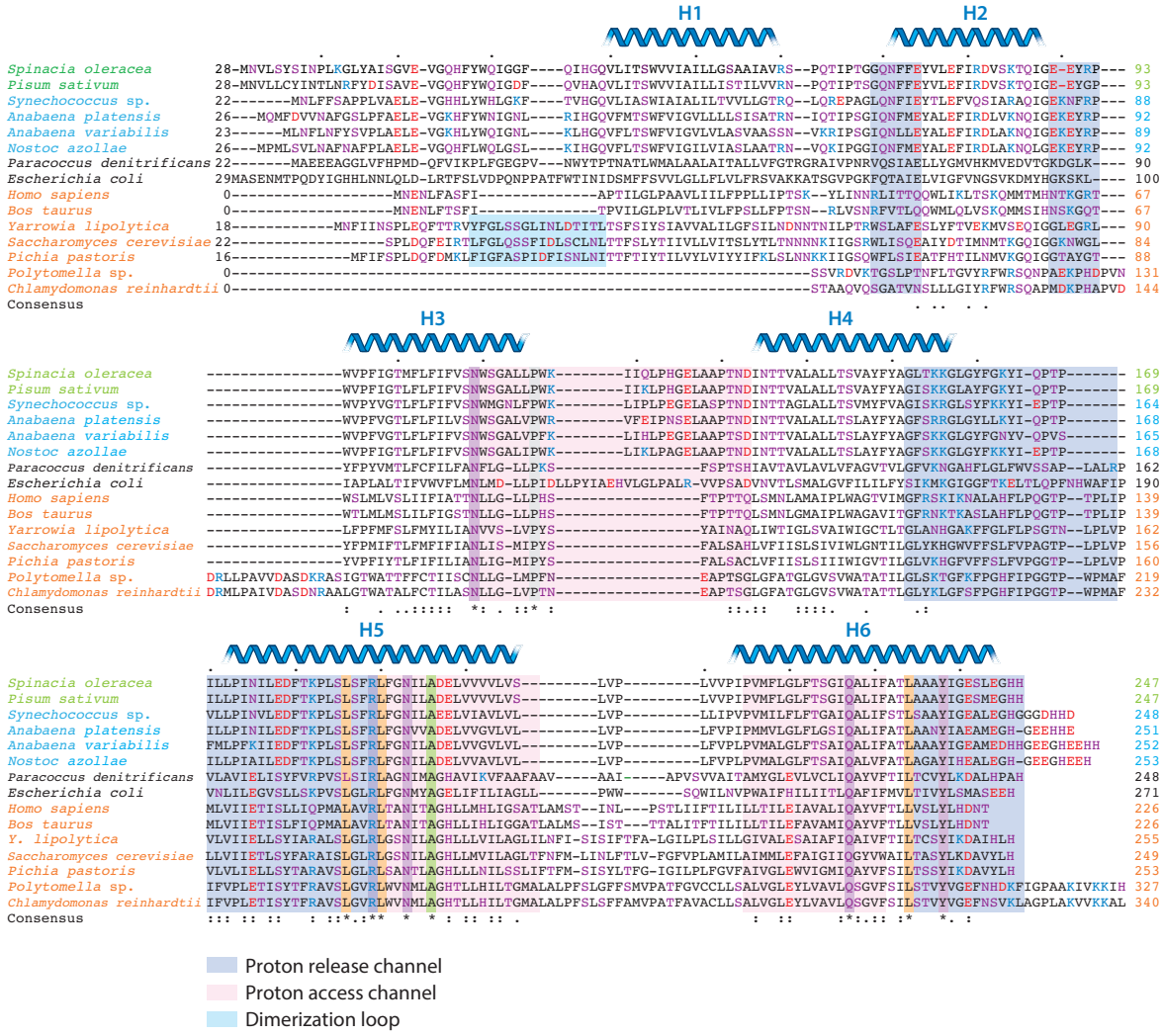

Figure 10

Structure-based sequence alignment of subunit *a*. Polypeptide sequences of *a*-subunits from plants (*green*), cyanobacteria (*cyan*), bacteria (*black*), and mitochondria (*orange*) are highly conserved. Most *a*-subunits are 250 to 270 residues long and mitochondrially encoded, except those of unicellular green algae, which are nuclear encoded, with an ~100-residue mitochondrial targeting sequence that is cleaved off after import. Most have a membrane-spanning α-helix H1, followed by an amphipathic helix H2 on the matrix membrane surface. All of the 10 strictly conserved (*) and 44 highly conserved (:) residues are located in helices H3 to H6 that form two long, membrane-intrinsic helix hairpins (see **Figure 11**). Together with the *c*-ring and, in *Polytomella* sp., *ASA6*, the helices define two aqueous channels that each span half the membrane. Polar and charged residues in the regions shaded pink define the proton access channel. The proton release channel is lined by polar and charged residues in the regions shaded blue. The structure of the *Saccharomyces cerevisiae* F_o dimer (78) indicates a loop near the N-terminal end of H1 (*light blue*) that is conserved in fungal ATP synthases. Together with subunit *i*, the *a*-subunit loop participates directly in the formation of mitochondrial ATP synthase dimers. The loop is absent in mammals, accounting for the poor stability of bovine ATP synthase dimers. Plant and bacterial ATP synthases do not have these subunits and do not form dimers. Residue color code: negatively charged (*red*); positively charged (*blue*); uncharged polar (*purple*). Colored bands highlight the 10 strictly conserved residues by type: uncharged polar (*purple*); proline (*gray*); large hydrophobic (*orange*); small hydrophobic (*green*). The essential arginine is blue.

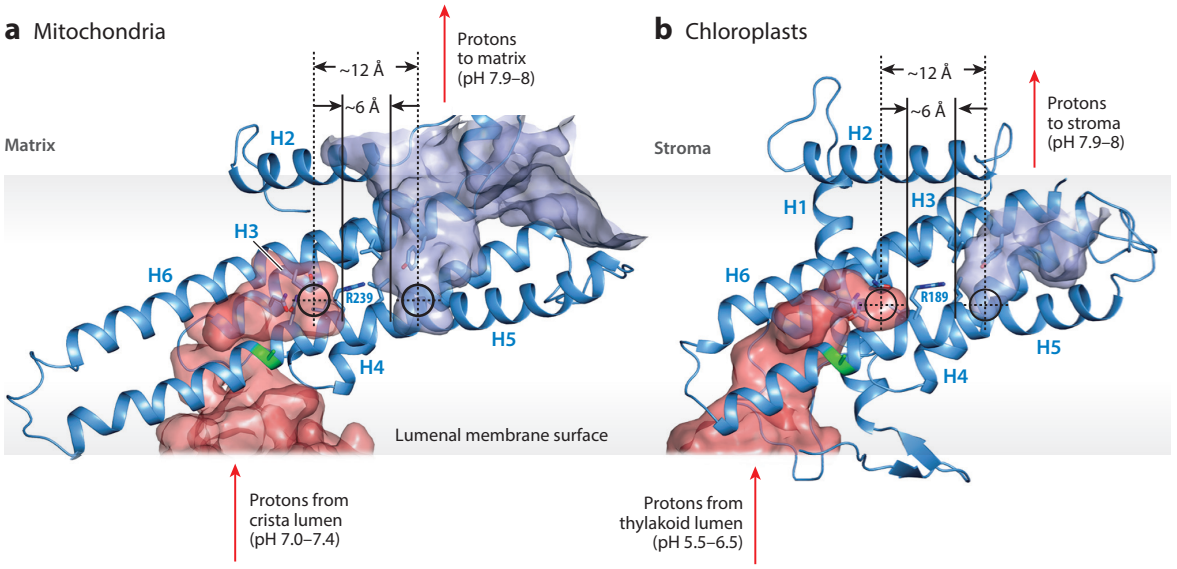

Figure 11

Proton access and release channels in subunit *a*. The structures of proton access channels (*transparent pink*) and release channels (*transparent blue*) in subunit *a* of (*a*) *Polytomella* mitochondria (80) and (*b*) Spinach chloroplasts (48) are conserved. Aqueous cavities are lined by polar and charged residues (**Figure 10**) in the long, membrane-intrinsic hairpins of H3/H4 and H5/H6 (*light blue*). Channels are viewed from the direction of the *c*-ring rotor. Cross-wire targets mark the position of glutamates in adjacent *c*-ring subunits. The ~12-Å conserved center-to-center distance between the access and exit channels matches the distance between *c*-ring protonation sites (**Figure 9**). Strictly conserved residues in H3, H5, and H6 (**Figure 10**) are drawn in stick representation. Two asparagines (Asn163 and Asn243 in *Polytomella*, Asn109 and Asn193 in Spinach) and a glutamine (Gln295 in *Polytomella*, Gln227 in Spinach) form a cluster that creates a hydrophilic environment at the end of the access channel. A conserved tyrosine (Tyr306 in *Polytomella*, Tyr238 in Spinach) performs the same role in the exit channel. The conserved alanine (*green*) marks the narrow gap between H5 and H6 for the access channel and ensures close contact to the *c*-ring. After an almost full *c*-ring rotation, the protonated glutamates encounter the release channel. Protons are siphoned off to the high pH of the mitochondrial matrix or chloroplast stroma via the conserved tyrosine in the exit channel. Access and release channels are separated by the strictly conserved arginine in H5. The ~6-Å edge-to-edge distance between access and release channels creates a strong electrostatic field parallel to the membrane plane that promotes *c*-ring rotation from left to right in synthesis mode.

the lumenal side to the protonated *c*-ring glutamate and a release channel from the glutamate of the adjacent *c*-ring subunit to the mitochondrial matrix or chloroplast stroma (**Figure 11**). The two channels are lined by the conserved polar and charged residues in H3 to H6 (**Figure 10**). Each channel spans half the membrane, as first postulated in 1994 on the basis of *E. coli* double mutants (120). The access channel turns ~90° halfway through the membrane and passes through a narrow gap in the long H5/H6 hairpin at a constriction of 5 × 6 Å created by small hydrophobic side chains (48, 80, 81) (**Figure 11**). The H5/H6 hairpin appears to be essential for positioning the proton access channel against the passing *c*-ring glutamates, which would explain why it is so highly conserved (117). At the membrane surface, the proton release channel opens like a funnel, allowing the protons to escape from the *c*-ring glutamate to the mitochondrial matrix or chloroplast stroma (**Figure 11**).

In the hydrophobic core of F_o, the two channels are separated by the essential arginine in H5 (**Figures 10** and **11**). The positively charged, bulky side chain prevents proton leakage from the access channel to the release channel. It was thought that the arginine would form a salt bridge to the *c*-ring glutamate during rotary catalysis, or when the motor stalls. Three of the four

highest-resolution F_o structures (48, 78, 80, 81) do not support such a salt bridge in the resting state, although it may form transiently during rotation between substates.

Mechanism of Proton Translocation and Torque Generation in F_o

Without a detailed structure of the F_o motor, insights into proton translocation and how it drives ATP synthesis had remained sketchy and speculative. The recent high-resolution cryo-EM maps of chloroplast and mitochondrial ATP synthases (48, 76, 78, 80, 81) (**Table 1**) all show essentially the same F_o structure and provide a firm base for a detailed description of proton translocation and torque generation: Protons from the *a*-subunit access channel protonate the glutamate (or aspartate in *E. coli*) in the ion-binding site of the proximal *c*-ring subunit, neutralizing its negative charge. The protonated, uncharged side chain partitions into the hydrophobic membrane environment, moving in counterclockwise direction as seen from the matrix or stroma. This puts the glutamate of the following *c*-ring subunit next to the access channel. After a rotation by $(n - 1)$ subunits (where n is the number of subunits in the ring), the protonated glutamate encounters the proton release channel and the proton is pulled off by the high pH of the mitochondrial matrix or chloroplast stroma (**Figure 11**; **Supplemental Video 5**).

Supplemental Material >

Glutamate or aspartate side chains are rarely visible in cryo-EM structures (20, 121), because their carboxyl groups are particularly sensitive to radiation damage and tend to be lost first during electron irradiation (121, 122). High-resolution X-ray structures of isolated *c*-rings show the glutamate in either a closed, ion-locked state (27, 108, 123) or an open conformation (124). Biochemical evidence and molecular dynamics simulations (125) suggest that the deprotonated glutamate is in the open conformation when it encounters the proton access channel and converts to the ion-locked state upon protonation.

The center-to-center distance between the proton access and release channels at the level of the *c*-ring glutamates is 12–13 Å in both *Polytomella* (**Figure 11*a***) and cF_1F_o (**Figure 11*b***). This distance matches the ~12 Å spacing between the protonatable glutamates of adjacent ring subunits (**Figure 9**). The spacing of glutamate β-carbons is slightly larger in small *c*-rings (12.8 Å for c_8) and slightly smaller in large rings (11.4 Å for c_{14}) but is always within a range that enables the simultaneous protonation of one glutamate and deprotonation of the next glutamate in the ring. H5 of subunit *a* bends around the *c*-ring, following its curvature as a hydrophobic bearing. In this way, *a*-subunits can accommodate rotor rings of diameters ranging from 38 Å to 62 Å or more (**Figure 9**). A similarly adaptable arrangement would be hard to achieve and maintain over long evolutionary timescales with standard transmembrane helices.

The proton-motive force (pmf) that drives ATP synthesis in mitochondria and chloroplasts is roughly the same—up to −210 mV in mitochondria (126) or −180 mV in chloroplasts (127). The pmf has a more or less stable electrostatic component $\Delta\psi$ and a ΔpH component that varies with the proton gradient across the membrane. The two components are thermodynamically equivalent. In mitochondria, $\Delta\psi$ is approximately −150 mV, whereas ΔpH is less than −60 mV (<1 pH unit). In chloroplasts, $\Delta\psi$ is approximately −30 mV (128), whereas ΔpH rises to −150 mV (2.5 pH units) in high light. The pmf exerts a force on the deprotonated, negatively charged glutamates of the *c*-ring (**Figure 12**). The force produced by a −200 mV potential across a 35-Å membrane (**Figure 12*c***) would be roughly 2.3 pN·nm, assuming a dielectric constant of 4 in the protein interior (129, 130). However, this force not only is too small but also has the wrong direction (perpendicular to the membrane plane) to generate torque and drive *c*-ring rotation. A higher force in the required direction tangential to the *c*-ring results when the distance between the proton access and exit channels in subunit *a* is taken into account (**Figures 11** and **12*d***). The ~6-Å edge-to-edge distance between channels generates a local field and consequently a force

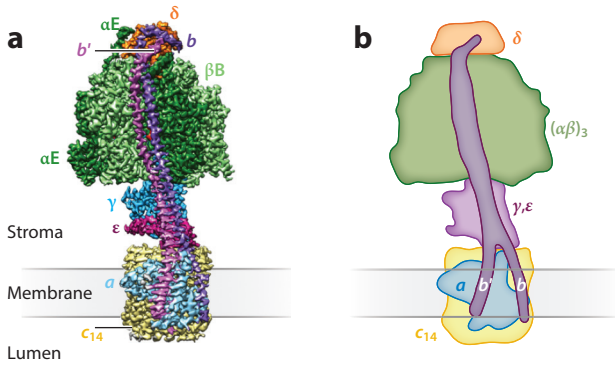

Figure 12

(*Figure continued on next page*)

that would be six times stronger. The force on the negatively charged glutamate translates into a torque of 36 pN·nm at the 2.7-nm radius of the chloroplast c_{14} ring (**Figure 12*e***). For mitochondria, the smaller radius of the c_{10} or c_8 ring (2.2 or 1.9 nm) would result in a smaller torque of 29 or 25 pN·nm. Considering the large error margin on the protein dielectric, these values are consistent with the 40–60 pN·nm torque determined in single-molecule experiments with immobilized bacterial F_1 heads (131–133).

The free energy ΔG of ATP hydrolysis under physiological conditions is approximately −50 kJ/mol. Given that ATP synthases operate reversibly close to thermodynamic equilibrium, each translocated proton provides $-50 \times 3/14$ or −10.7 kJ/mol to ATP synthesis in chloroplasts but almost twice as much (−18.7 kJ/mol) in mammalian mitochondria. This surprising discrepancy may be explained by the variable pmf in chloroplasts as compared to the stable pmf in mitochondria. ΔpH in chloroplasts fluctuates with light intensity, and it might therefore be an advantage to have a larger number of *c*-ring subunits in the ring that each make a smaller contribution, to maintain ATP synthesis in low light.

The conserved small distance between the proton access and release channels in subunit *a* supports the notion that the force of the electrostatic field acting on the deprotonated glutamate facilitates directional *c*-ring rotation (134). An earlier model of rotary ATPases (135) that was based on two hypothetical, laterally displaced half channels (120) is not inconsistent with this mechanism. In the earlier model, torque is generated by stochastic bidirectional oscillations of the rotor, biased by the free energy of the pmf, which is sufficient to explain directional rotation. The pmf ultimately determines the driving force in all possible mechanisms, but the well-placed directional force on the charged *c*-ring glutamate helps to overcome the activation barrier and to move the *c*-ring past the gating *a*-subunit arginine. The local electrostatic force is likely to offer a significant kinetic advantage for a process that has to occur thousands of times per second.

Mitochondrial ATP Synthase Dimers and Membrane Curvature

Formation of Type I dimers depends on the dimer-specific subunits *e*, *g*, and *k* (55, 61, 82). Contrary to expectation, these subunits do not interact directly at the dimer interface (78, 79). Rather, they form a hydrophobic wedge on either side of the dimer (**Figure 6*b***) that imposes a local curvature on the membrane, even in monomers (79, 136, 137). In yeasts, an extended loop of subunit *a* (**Figures 6*b*** and **10**) establishes direct dimer contacts, together with subunit *j* (78). In mammalian mitochondria, *j* is replaced by a subunit termed *6.8PL* (95), and the *a*-subunit loop is missing (**Figure 10**), which accounts for the poor stability of the bovine dimer.

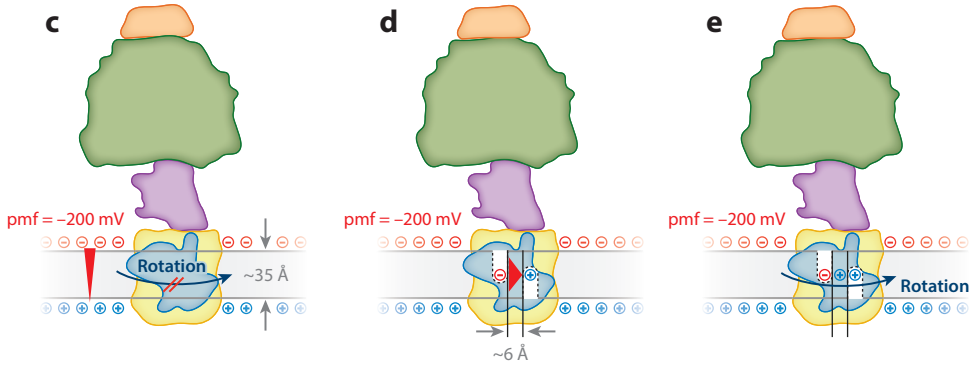

Figure 12

Torque generation in F-type ATP synthases. (*a*) Cryo-EM map of chloroplast ATP synthase (48) in the membrane (*gray*). (*b*) Schematic of main components. (*c*) The lumenal membrane surface is negatively charged, and the stromal surface is positively charged. The proton-motive force (pmf) of −200 mV exerts a force perpendicular to the membrane plane (*narrow red arrowhead*) on the deprotonated glutamates in the *c*-ring. A force in this direction does not generate torque and cannot drive *c*-ring rotation (*blue arrow*). (*d*) The ~6-Å edge-to-edge distance between the proton access and release channels (see **Figure 11**) generates a field parallel to the membrane plane that is approximately six times stronger (*wide red arrowhead*). (*e*) The strong field promotes *c*-ring rotation in the indicated direction (synthesis mode), driving ATP synthesis in the F_1 head. In panels *c*–*e*, the peripheral stalk is omitted for clarity.

Dimer ribbons form spontaneously upon lipid reconstitution of purified *Y. lipolytica* Type I and *Polytomella* Type II dimers (68) (**Figure 13**; **Supplemental Video 6**). Computer simulations indicate that row formation is driven by the elastic energy of membrane deformation (61, 138). Insertion of one dimeric complex with a dimer angle of 90° or 56° into a planar lipid bilayer induces high local membrane curvature. The next inserted dimer would then diffuse to a position adjacent to the first dimer to minimize the overall bending energy, and so on for subsequent dimers. This results in the formation of rows or ribbons without the need for specific protein–protein contacts.

Supplemental Material >

The assembly of mtF_1F_o dimers into rows is a universal feature of all known mitochondrial ATPases. Type II and IV dimers form short helical ribbons that wrap around the edges of club-shaped or disk-like cristae (**Figure 5*f*,*h***). Type III dimers of ciliates associate into extensive, closely spaced helical rows that give rise to tubular cristae (71). No apparent sequence or structural similarity exists between the subunits involved in the formation of Type I and Type II dimers. The fact that the dimers are ubiquitous in mitochondria of all organisms and are, as an entity, more highly conserved than the subunits involved in their formation proves that they are fundamentally important.

Cristae Formation

The inner membrane cristae in mitochondria are intimately linked to mtF_1F_o dimers. In *S. cerevisiae*, *Y. lipolytica*, or bovine mitochondria, Type I mtF_1F_o dimers assemble into rows of more than 1 μm in length (59, 61) at the tightly curved edges of lamellar cristae (**Figures 5*e*** and **13**; **Supplemental Video 1**). Conventional electron microscopy of yeast Δ*e* and Δ*g* mutants revealed onion-like concentric inner membrane layers instead of normal lamellar cristae (82). Cryo-ET of mitochondria isolated from Δ*e* and Δ*g* mutants indicated the absence of mtF_1F_o dimers or lamellar cristae and the presence of randomly distributed mtF_1F_o monomers in the membrane (61). In mitochondria of *Podospora anserina*, a fungal model organism of cellular aging, cryo-ET of mitochondria from young cultures indicated normal lamellar cristae and dimer rows but no

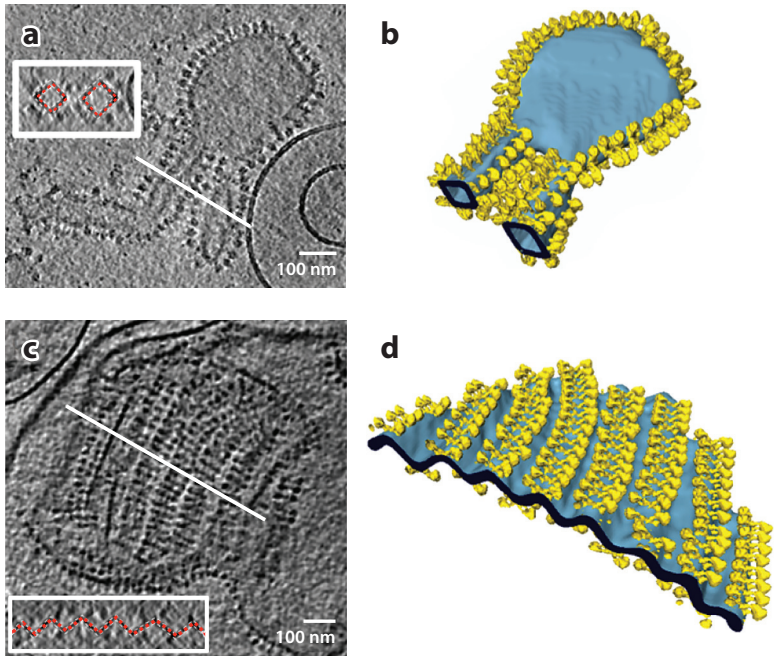

Figure 13

Cryo-ET shows that ATP synthase dimers reconstituted into liposomes self-assemble into rows and bend the membrane. (*a*) Section through tomographic volume of lipid vesicle with rows of membrane-inserted *Yarrowia lipolytica* ATP synthase dimers around the edge. Cross sections (*white lines*, *insets*) indicate that the dimer rows bend the lipid bilayer by ~90° (*dashed red lines*). (*b*) The 3D-rendered volume indicates that ATP synthase dimers (*yellow*) spontaneously assemble into rows at the tightly curved vesicle edges, as in mitochondrial cristae (see **Figure 5*e***; **Supplemental Video 1**). ATP synthase is absent from flat membrane regions (*light blue*). (*c*,*d*) Parallel rows of bidirectionally inserted dimers (*yellow*) bend the lipid bilayer (*light blue*) into a corrugated sheet. See also **Supplemental Video 6**. Figure adapted from Reference 68.

Supplemental Material >

monomers (62). In aging cells, the dimers began to break up. In old cells, all dimers had dissociated into monomers and the lamellar cristae had turned into balloon-shaped vesicles. Both cryo-ET studies demonstrate that cristae formation depends on mtF_1F_o dimers and dimer rows.

An obvious effect of the cristae, and hence of ATP synthase dimers, is that they increase the surface area of the inner mitochondrial membrane. A rough estimate shows that, for a cylindrical mitochondrion of radius r and infinite length, stacked with lamellar cristae at a repeat distance d, the surface area increases by a factor of $(r/d + 1)$. Assuming a radius of 350 nm and a lamellar stacking distance of 41 nm [both typical for mouse heart mitochondria (139)], the membrane surface area increases approximately ten-fold, compared with an inner membrane cylinder without cristae. The extra membrane surface can accommodate ten times more respiratory chain and other protein complexes. Mitochondria from other tissues are less tightly packed (139), and the surface increase is correspondingly smaller.

But to enlarge the membrane surface area is not the only, and almost certainly not the main, effect of the cristae. Yeast Δe and Δg mutants do not have dimers and have no regular cristae, yet compared with wild type, the total inner membrane surface does not appear conspicuously reduced (61, 82). A more striking difference is that the mutants grow up to 60% more slowly. Their mitochondrial membrane potential has been reported to drop by 80% (140), although this has not been confirmed by another study (141). The reduced membrane potential, and therefore

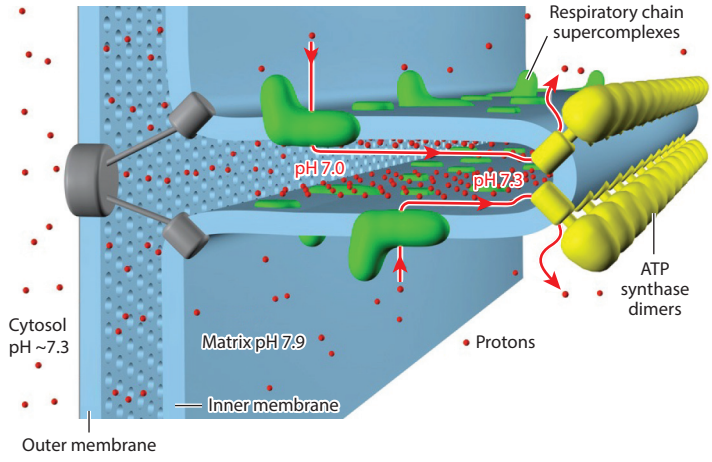

Figure 14

ATP synthase dimers and respiratory chain complexes in mitochondrial cristae. ATP synthase dimers (*yellow*) and respiratory chain complexes (*green*) are laterally segregated and occupy different membrane regions. Mitochondrial ATP synthase forms dimer rows at the cristae ridges, whereas the proton pumps of the electron transfer chain reside in the adjacent, continuous planar membranes (142). The local pH on the lumenal side of respiratory chain complex IV and ATP synthase has been determined ratiometrically (143). Protons (*red*) pumped into the cristae space by the electron transport complexes flow back into the matrix through F_o, driving ATP synthesis. The mitochondrial outer membrane is porous to small molecules and ions, including protons. The gray complex that connects inner and outer membranes at the cristae junctions is hypothetical. Figure adapted from Reference 60.

pmf, may be related to the 3D membrane architecture and spatial segregation of respiratory chain complexes or supercomplexes (142) and ATP synthase dimer rows (**Figure 14**). Cristae are microcompartments that may work as proton traps. When the dimers dissociate, the cristae unfold (61, 62), the protons escape, and the pmf dissipates. By contrast, protons cannot easily escape from chloroplast thylakoids, because the thylakoid membrane is a closed system without an outlet to the intermembrane space. The sealed, proton-tight vesicles safeguard the high pH gradient of up to 2.5 units across the thylakoid membrane (127), whereas the small proton gradient of no more than 0.6 to 0.8 pH units across the mitochondrial inner membrane (143, 144) must be protected. The ATP synthase dimer rows and their capacity to shape the inner mitochondrial membrane into cristae appear to do exactly that.

A recent analysis revealed that, surprisingly, germline stem cell differentiation in *Drosophila* depended on cristae formation. The mitochondrial ATP synthase itself was critical, whereas ATP synthesis or oxidative phosphorylation was not (145). Stem cell differentiation required the specific upregulation of ATP synthase expression and formation of ATP synthase dimers, as differentiation was impaired in subunit *e* and *g* knockdowns (145). The cellular and molecular mechanisms behind these processes are unknown.

ATP Synthase and Health

Many severe neuromuscular, neurodevelopmental, and neurodegenerative diseases are linked to mitochondria. Of these mitochondrial disorders, 48 have been traced to mutations in subunit *a* (*ATP6*, *MT-ATP6*, or *Atp6p* in the medical literature) and 14 to subunit *8* (*A6L*, *ATP8*, *MT-ATP8*, or *Atp8p*) (see Reference 94 for a comprehensive recent review). Both subunits are among

the 13 human proteins encoded by mitochondrial DNA (mtDNA). Several of the most serious defects map to the proton release channel, or they disrupt H5 of subunit *a* and hence impair F_o stability (80, 94). The resulting disorders are maternally inherited and incurable. At present, the potential for medical intervention seems remote, because each cell has a thousand or more copies of mtDNA. But knowing the exact location of the mutated residues at least in a model organism (76, 78, 79) will help to explore their role in the function and stability of the complex, as an important first step toward the development of future therapies.

In view of their central role in cellular energy metabolism and clear differences in structure, sequence, and subunit composition compared with human mtF_1F_o, the ATP synthases of pathogenic organisms are excellent drug targets, especially for much-needed antibiotics against multidrug-resistant strains. The 1.7-Å X-ray structure of the c_9 rotor ring from *Mycobacterium phlei*, a nonpathogenic relative of *Mycobacterium tuberculosis*, in complex with the new antibiotic bedaquiline (146) shows how the drug interacts with the proton-binding site of the *c*-ring subunit. Bedaquiline is the first compound in 40 years to be approved for treatment of multidrug-resistant tuberculosis. This approach paves the way for the development of new compounds that act against *M. tuberculosis* and other human pathogens. Similarly, the characteristic pyramidal structure of the trypanosomal F_1 head with its unique *p18* subunit (72, 73) may prove a suitable target for developing new drugs against sleeping sickness.

FUTURE ISSUES

1. It will be important to determine the high-resolution structure of a mammalian, preferably the human, mtF_1F_o. The unconventional Type III or Type IV mtF_1F_o dimers are interesting for structural studies in their own right while also being potential drug targets against protozoan pathogens.
2. Cryo-EM and X-ray crystallography provide detailed snapshots of the molecular machinery that translocates protons and generates ATP, but static structures alone cannot explain the ATP synthase mechanisms fully. Molecular dynamics simulations of the entire complex on a timescale of milliseconds will be necessary to understand these processes at the atomistic level. With the continuing rapid increase in computer power, such demanding calculations should soon come into reach.
3. The role of mitochondrial ATP synthase dimers in cellular physiology is not understood. Clearly, the dimers are responsible for cristae formation (61, 82), but why are the cristae so important? Do they help to maintain the membrane potential? What is their significance in the development of multicellular organisms (145)?
4. The role of mtF_1F_o dimers in aging needs to be investigated further. It is known from one model organism that dimers dissociate and the inner membrane vesiculates in old cells (62), but it is not known whether this is a cause or an effect of aging or whether the observed age-related changes in mouse mitochondria (139) result from the same process.
5. Mitochondrial ATP synthase dimers have been implicated in the formation of the mitochondrial permeability transition pore (104) that causes a sudden swelling of mitochondria in vitro or during cardiac arrest, leading to membrane rupture and apoptosis. The molecular events behind this phenomenon have proved elusive in decades of research. More work is required to establish whether ATP synthase dimers play a role and, if so, how they are involved.

6. The biogenesis of ATP synthases is insufficiently explored. F_1F_o assembly in mitochondria and chloroplasts requires the precise coordination of organellar and nuclear gene expression. A number of key assembly intermediates and factors have been identified (95, 147). Super-resolution light microscopy indicates that the assembly of the mitochondrial complex takes place in the cristae rather than in the boundary membrane (148), but how F_1F_o assembly is synchronized, what signals are transmitted, and how the components get to their destination in the membrane are largely unknown.
7. An unresolved—and most likely unresolvable—mystery of the ATP synthase is that of its evolutionary origins. It is clear from the conserved mechanisms and structure of mitochondrial and chloroplast ATPases that they predate the divergence of these lineages 1.5 billion years ago (91, 92). The fact that the mechanisms of proton translocation and ATP synthesis have remained unchanged ever since is astonishing in itself. Evidently, not even small changes in essential residues are tolerated. There are good reasons to think that the ATP synthase, along with the ribosome, is one of the two most ancient macromolecular machines in biology (149). Rotary ATP synthases must have existed in the bacterial precursors of mitochondria and chloroplasts, but how and where did they originate? Speculation abounds (150, 151) but is necessarily inconclusive.

DISCLOSURE STATEMENT

The author is not aware of any affiliations, memberships, funding, or financial holdings that might be perceived as affecting the objectivity of this review.

ACKNOWLEDGMENTS

I thank Bonnie Murphy, Janet Vonck, Alexander Hahn, and Thomas Meier for their suggestions and critical comments on the manuscript. Janet Vonck carried out the *δ/OSCP* and *a*-subunit alignments. Alexander Hahn drew **Figures 7** and **8**. Özkan Yildiz helped to draw **Figures 4*b*** and **11**. Paolo Lastrico is acknowledged for expert graphics assistance. Bertram Daum, Karen Davies, Niklas Klusch, Bonnie Murphy, and Alexander Hahn contributed the **Supplemental Videos**. This work was supported by the Max Planck Society.

LITERATURE CITED

1. von Ballmoos C, Wiedenmann A, Dimroth P. 2009. Essentials for ATP synthesis by F_1F_o ATP synthases. *Annu. Rev. Biochem.* 78:649–72
2. Junge W, Nelson N. 2015. ATP synthase. *Annu. Rev. Biochem.* 84:631–57
3. Walker JE. 2013. The ATP synthase: the understood, the uncertain and the unknown. *Biochem. Soc. Trans.* 41:1–16
4. Kagawa Y, Racker E. 1966. Partial resolution of the enzymes catalyzing oxidative phosphorylation. X. Correlation of morphology and function in submitochondrial particles. *J. Biol. Chem.* 241:2475–82
5. Penefsky HS, Pullman ME, Datta A, Racker E. 1960. Partial resolution of the enzymes catalyzing oxidative phosphorylation. II. Participation of a soluble adenosine triphosphatase in oxidative phosphorylation. *J. Biol. Chem.* 235:3330–36
6. Boyer PD. 1997. The ATP synthase—a splendid molecular machine. *Annu. Rev. Biochem.* 66:717–49
7. Boyer PD, Chance B, Ernster L, Mitchell P, Racker E, Slater EC. 1977. Oxidative phosphorylation and photophosphorylation. *Annu. Rev. Biochem.* 46:955–1026

8. Walker JE. 1998. ATP synthesis by rotary catalysis (Nobel lecture). *Angew. Chem. Int. Ed. Engl.* 37:2308–19
9. Nakamoto RK, Scanlon JAB, Al-Shawi MK. 2008. The rotary mechanism of the ATP synthase. *Arch. Biochem. Biophys.* 476:43–50
10. Forgac M. 2007. Vacuolar ATPases: rotary proton pumps in physiology and pathophysiology. *Nat. Rev. Mol. Cell Biol.* 8:917–29
11. Müller V, Grüber G. 2003. ATP synthases: structure, function and evolution of unique energy converters. *Cell. Mol. Life Sci.* 60:474–94
12. Wienisch M, Klingauf J. 2006. Vesicular proteins exocytosed and subsequently retrieved by compensatory endocytosis are nonidentical. *Nat. Neurosci.* 9:1019–27
13. Ohya Y, Umemoto N, Tanida I, Ohta A, Iida H, Anraku Y. 1991. Calcium-sensitive *cls* mutants of *Saccharomyces cerevisiae* showing a Pet^- phenotype are ascribable to defects of vacuolar membrane H^+-ATPase activity. *J. Biol. Chem.* 266:13971–77
14. Grüber G, Manimekalai MS, Mayer F, Müller V. 2014. ATP synthases from archaea: the beauty of a molecular motor. *Biochim. Biophys. Acta* 1837:940–52
15. Kühlbrandt W. 2014. The resolution revolution. *Science* 343:1443–44
16. Zhang X, Jin L, Fang Q, Hui WH, Zhou ZH. 2010. 3.3 Å cryo-EM structure of a nonenveloped virus reveals a priming mechanism for cell entry. *Cell* 141:472–82
17. Grigorieff N, Harrison SC. 2011. Near-atomic resolution reconstructions of icosahedral viruses from electron cryo-microscopy. *Curr. Opin. Struct. Biol.* 21:265–73
18. Mills DJ, Vitt S, Strauss M, Shima S, Vonck J. 2013. De novo modeling of the F_{420}-reducing [NiFe]-hydrogenase from a methanogenic archaeon by cryo-electron microscopy. *eLife* 2:e00218
19. Henderson R, Baldwin JM, Ceska TA, Zemlin F, Beckmann E, Downing KH. 1990. A model for the structure of bacteriorhodopsin based on high resolution electron cryo-microscopy. *J. Mol. Biol.* 213:899–929
20. Kühlbrandt W, Wang DN, Fujiyoshi Y. 1994. Atomic model of plant light-harvesting complex by electron crystallography. *Nature* 367:614–21
21. Murata K, Mitsuoka K, Hirai T, Walz T, Agre P, et al. 2000. Structural determinants of water permeation through aquaporin-1. *Nature* 407:599–605
22. Faruqi AR, Henderson R. 2007. Electronic detectors for electron microscopy. *Curr. Opin. Struct. Biol.* 17:549–55
23. Scheres SH. 2012. RELION: implementation of a Bayesian approach to cryo-EM structure determination. *J. Struct. Biol.* 180:519–30
24. Abrahams JP, Leslie AG, Lutter R, Walker JE. 1994. Structure at 2.8 Å resolution of F_1-ATPase from bovine heart mitochondria. *Nature* 370:621–28
25. Stock D, Leslie AGW, Walker JE. 1999. Molecular architecture of the rotary motor in ATP synthase. *Science* 286:1700–5
26. Dickson VK, Silvester JA, Fearnley IM, Leslie AG, Walker JE. 2006. On the structure of the stator of the mitochondrial ATP synthase. *EMBO J.* 25:2911–18
27. Meier T, Polzer P, Diederichs K, Welte W, Dimroth P. 2005. Structure of the rotor ring of F-type Na^+-ATPase from *Ilyobacter tartaricus*. *Science* 308:659–62
28. Rubinstein JL, Walker JE, Henderson R. 2003. Structure of the mitochondrial ATP synthase by electron cryomicroscopy. *EMBO J.* 22:6182–92
29. Schur FKM, Obr M, Hagen WJH, Wan W, Jakobi AJ, et al. 2016. An atomic model of HIV-1 capsid-SP1 reveals structures regulating assembly and maturation. *Science* 353:506–8
30. Parsons DF. 1963. Mitochondrial structure: two types of subunits on negatively stained mitochondrial membranes. *Science* 140:985–87
31. Wilkens S, Capaldi RA. 1998. ATP synthase's second stalk comes into focus. *Nature* 393:29
32. Dimroth P. 1997. Primary sodium ion translocating enzymes. *Biochim. Biophys. Acta* 1318:11–51
33. Krah A, Pogoryelov D, Langer JD, Bond PJ, Meier T, Faraldo-Gomez JD. 2010. Structural and energetic basis for H^+ versus Na^+ binding selectivity in ATP synthase F_o rotors. *Biochim. Biophys. Acta* 1797:763–72

34. Fillingame RH, Steed PR. 2014. Half-channels mediating H transport and the mechanism of gating in the F_o sector of *Escherichia coli* F_1F_o ATP synthase. *Biochim. Biophys. Acta* 1837:1063–68
35. Steed PR, Kraft KA, Fillingame RH. 2014. Interacting cytoplasmic loops of subunits *a* and *c* of *Escherichia coli* F_1F_o ATP synthase gate H^+ transport to the cytoplasm. *PNAS* 111:16730–35
36. Jiang W, Fillingame RH. 1998. Interacting helical faces of subunits *a* and *c* in the F_1F_o ATP synthase of *Escherichia coli* defined by disulfide cross-linking. *PNAS* 95:6607–12
37. Vik SB, Dao NN. 1992. Prediction of transmembrane topology of F_o proteins from *Escherichia coli* F_1F_o ATP synthase using variational and hydrophobic moment analyses. *Biochim. Biophys. Acta* 1140:199–207
38. Lightowlers RN, Howitt SM, Hatch L, Gibson F, Cox GB. 1987. The proton pore in the *Escherichia coli* F_oF_1-ATPase: a requirement for arginine at position 210 of the *a*-subunit. *Biochim. Biophys. Acta* 894:399–406
39. Howitt SM, Cox GB. 1992. Second-site revertants of an arginine-210 to lysine mutation in the *a*-subunit of the F_oF_1-ATPase from *Escherichia-coli*: implications for structure. *PNAS* 89:9799–803
40. Weber J, Senior AE. 1997. Catalytic mechanism of F_1-ATPase. *Biochim. Biophys. Acta* 1319:19–58
41. Futai M, Omote H, Sambongi Y, Wada Y. 2000. Synthase (H^+ ATPase): coupling between catalysis, mechanical work, and proton translocation. *Biochim. Biophys. Acta* 1458:276–88
42. Wächter A, Bi Y, Dunn SD, Cain BD, Sielaff H, et al. 2011. Two rotary motors in F-ATP synthase are elastically coupled by a flexible rotor and a stiff stator stalk. *PNAS* 108:3924–29
43. Noji H, Yasuda R, Yoshida M, Kinosita K Jr. 1997. Direct observation of the rotation of F_1-ATPase. *Nature* 386:299–302
44. Yasuda R, Noji H, Yoshida M, Kinosita K Jr., Itoh H. 2001. Resolution of distinct rotational substeps by submillisecond kinetic analysis of F_1-ATPase. *Nature* 410:898–904
45. Fischer S, Etzold C, Turina P, Deckershebestreit G, Altendorf K, Gräber P. 1994. ATP synthesis catalyzed by the ATP synthase of *Escherichia coli* reconstituted into liposomes. *Eur. J. Biochem.* 225:167–72
46. Sobti M, Smits C, Wong AS, Ishmukhametov R, Stock D, et al. 2016. Cryo-EM structures of the autoinhibited *E. coli* ATP synthase in three rotational states. *eLife* 5:e21598
46a. Sobti M, Ishmukhametov R, Bouwer JC, Ayer A, Suarna C, et al. 2019. Cryo-EM reveals distinct conformations of *E. coli* ATP synthase on exposure to ATP. *eLife* 8:e43864
47. Guo H, Suzuki T, Rubinstein JL. 2019. Structure of a bacterial ATP synthase. *eLife* 8:e43128
48. Hahn A, Vonck J, Mills DJ, Meier T, Kühlbrandt W. 2018. Structure, mechanism, and regulation of the chloroplast ATP synthase. *Science* 360:eaat4318
49. Cingolani G, Duncan TM. 2011. Structure of the ATP synthase catalytic complex (F_1) from *Escherichia coli* in an autoinhibited conformation. *Nat. Struct. Mol. Biol.* 18:701–7
50. Morales-Rios E, Montgomery MG, Leslie AG, Walker JE. 2015. Structure of ATP synthase from *Paracoccus denitrificans* determined by X-ray crystallography at 4.0 Å resolution. *PNAS* 112:13231–36
51. Böttcher B, Gräber P. 2000. The structure of the H^+-ATP synthase from chloroplasts and its subcomplexes as revealed by electron microscopy. *Biochim. Biophys. Acta* 1458:404–16
52. Mellwig C, Böttcher B. 2003. A unique resting position of the ATP-synthase from chloroplasts. *J. Biol. Chem.* 278:18544–49
53. Daum B, Nicastro D, Austin J 2nd, McIntosh JR, Kühlbrandt W. 2010. Arrangement of photosystem II and ATP synthase in chloroplast membranes of spinach and pea. *Plant Cell* 22:1299–312
54. Daum B, Kühlbrandt W. 2011. Electron tomography of plant thylakoid membranes. *J. Exp. Bot.* 62:2393–402
55. Arnold I, Pfeiffer K, Neupert W, Stuart RA, Schägger H. 1998. Yeast mitochondrial F_1F_o-ATP synthase exists as a dimer: identification of three dimer-specific subunits. *EMBO J.* 17:7170–78
56. Minauro-Sanmiguel F, Wilkens S, Garcia JJ. 2005. Structure of dimeric mitochondrial ATP synthase: novel F_o bridging features and the structural basis of mitochondrial cristae biogenesis. *PNAS* 102:12356–58
57. Dudkina NV, Heinemeyer J, Keegstra W, Boekema EJ, Braun HP. 2005. Structure of dimeric ATP synthase from mitochondria: an angular association of monomers induces the strong curvature of the inner membrane. *FEBS Lett.* 579:5769–72

58. Dudkina NV, Sunderhaus S, Braun HP, Boekema EJ. 2006. Characterization of dimeric ATP synthase and cristae membrane ultrastructure from *Saccharomyces* and *Polytomella* mitochondria. *FEBS Lett.* 580:3427–32
59. Strauss M, Hofhaus G, Schröder RR, Kühlbrandt W. 2008. Dimer ribbons of ATP synthase shape the inner mitochondrial membrane. *EMBO J.* 27:1154–60
60. Davies KM, Strauss M, Daum B, Kief JH, Osiewacz HD, et al. 2011. Macromolecular organization of ATP synthase and complex I in whole mitochondria. *PNAS* 108:14121–26
61. Davies KM, Anselmi C, Wittig I, Faraldo-Gomez JD, Kühlbrandt W. 2012. Structure of the yeast F_1F_o-ATP synthase dimer and its role in shaping the mitochondrial cristae. *PNAS* 109:13602–7
62. Daum B, Walter A, Horst A, Osiewacz HD, Kühlbrandt W. 2013. Age-dependent dissociation of ATP synthase dimers and loss of inner-membrane cristae in mitochondria. *PNAS* 110:15301–6
63. van Lis R, Gonzalez-Halphen D, Atteia A. 2005. Divergence of the mitochondrial electron transport chains from the green alga *Chlamydomonas reinhardtii* and its colorless close relative *Polytomella* sp. *Biochim. Biophys. Acta* 1708:23–34
64. van Lis R, Mendoza-Hernandez G, Groth G, Atteia A. 2007. New insights into the unique structure of the F_0F_1-ATP synthase from the chlamydomonad algae *Polytomella* sp. and *Chlamydomonas reinhardtii*. *Plant Physiol.* 144:1190–99
65. Vazquez-Acevedo M, Cardol P, Cano-Estrada A, Lapaille M, Remacle C, Gonzalez-Halphen D. 2006. The mitochondrial ATP synthase of chlorophycean algae contains eight subunits of unknown origin involved in the formation of an atypical stator-stalk and in the dimerization of the complex. *J. Bioenerg. Biomembr.* 38:271–82
66. Cano-Estrada A, Vazquez-Acevedo M, Villavicencio-Queijeiro A, Figueroa-Martinez F, Miranda-Astudillo H, et al. 2010. Subunit–subunit interactions and overall topology of the dimeric mitochondrial ATP synthase of *Polytomella* sp. *Biochim. Biophys. Acta* 1797:1439–48
67. Dudkina NV, Oostergetel GT, Lewejohann D, Braun HP, Boekema EJ. 2010. Row-like organization of ATP synthase in intact mitochondria determined by cryo-electron tomography. *Biochim. Biophys. Acta* 1797:272–77
68. Blum TB, Hahn A, Meier T, Davies KM, Kühlbrandt W. 2019. Dimers of mitochondrial ATP synthase induce membrane curvature and self-assemble into rows. *PNAS* 116:4250–55
69. Vazquez-Acevedo M, Vega-deLuna F, Sanchez-Vasquez L, Colina-Tenorio L, Remacle C, et al. 2016. Dissecting the peripheral stalk of the mitochondrial ATP synthase of chlorophycean algae. *Biochim. Biophys. Acta* 1857:1183–90
70. Allen RD. 1995. Membrane tubulation and proton pumps. *Protoplasma* 189:1–8
71. Mühleip AW, Joos F, Wigge C, Frangakis AS, Kühlbrandt W, Davies KM. 2016. Helical arrays of U-shaped ATP synthase dimers form tubular cristae in ciliate mitochondria. *PNAS* 113:8442–47
72. Mühleip AW, Dewar CE, Schnaufer A, Kühlbrandt W, Davies KM. 2017. In situ structure of trypanosomal ATP synthase dimer reveals a unique arrangement of catalytic subunits. *PNAS* 114:992–97
73. Montgomery MG, Gahura O, Leslie AGW, Zikova A, Walker JE. 2018. ATP synthase from *Trypanosoma brucei* has an elaborated canonical F_1-domain and conventional catalytic sites. *PNAS* 115:2102–7
74. Davies KM, Kühlbrandt W. 2018. Structure of the catalytic F_1 head of the F_1F_o ATP synthase from *Trypanosoma brucei*. *PNAS* 115:E2906–7
75. Zhou A, Rohou A, Schep DG, Bason JV, Montgomery MG, et al. 2015. Structure and conformational states of the bovine mitochondrial ATP synthase by cryo-EM. *eLife* 4:e10180
76. Srivastava AP, Luo M, Zhou W, Symersky J, Bai D, et al. 2018. High-resolution cryo-EM analysis of the yeast ATP synthase in a lipid membrane. *Science* 360:eaas9699
77. Vinothkumar KR, Montgomery MG, Liu S, Walker JE. 2016. Structure of the mitochondrial ATP synthase from *Pichia angusta* determined by electron cryo-microscopy. *PNAS* 113:12709–14
78. Guo H, Bueler SA, Rubinstein JL. 2017. Atomic model for the dimeric F_o region of mitochondrial ATP synthase. *Science* 358:936–40
79. Hahn A, Parey K, Bublitz M, Mills DJ, Zickermann V, et al. 2016. Structure of a complete ATP synthase dimer reveals the molecular basis of inner mitochondrial membrane morphology. *Mol. Cell* 63:445–56

80. Klusch N, Murphy BJ, Mills DJ, Yildiz Ö, Kühlbrandt W. 2017. Structural basis of proton translocation and force generation in mitochondrial ATP synthase. *eLife* 6:e33274
81. Murphy BJ, Klusch N, Langer JD, Mills DJ, Yildiz Ö, Kühlbrandt W. 2019. Rotary substates of mitochondrial ATP synthase reveal the basis of flexible F_1-F_o coupling. *Science*. In press. **https://doi.org/10.1126/science.aaw9128**
82. Paumard P, Vaillier J, Coulary B, Schaeffer J, Soubannier V, et al. 2002. The ATP synthase is involved in generating mitochondrial cristae morphology. *EMBO J.* 21:221–30
83. Allegretti M, Klusch N, Mills DJ, Vonck J, Kühlbrandt W, Davies KM. 2015. Horizontal membrane-intrinsic α-helices in the stator *a*-subunit of an F-type ATP synthase. *Nature* 521:237–40
84. Symersky J, Osowski D, Walters DE, Mueller DM. 2012. Oligomycin frames a common drug-binding site in the ATP synthase. *PNAS* 109:13961–65
85. Martin JL, Ishmukhametov R, Spetzler D, Hornung T, Frasch WD. 2018. Elastic coupling power stroke mechanism of the F_1-ATPase molecular motor. *PNAS* 115:5750–55
86. Heineke D, Riens B, Grosse H, Hoferichter P, Peter U, et al. 1991. Redox transfer across the inner chloroplast envelope membrane. *Plant Physiol.* 95:1131–37
87. Yanagisawa S, Frasch WD. 2017. Protonation-dependent stepped rotation of the F-type ATP synthase c-ring observed by single-molecule measurements. *J. Biol. Chem.* 292:17093–100
88. Okazaki K, Hummer G. 2015. Elasticity, friction, and pathway of γ-subunit rotation in F_oF_1-ATP synthase. *PNAS* 112:10720–25
89. Wilkens S, Borchardt D, Weber J, Senior AE. 2005. Structural characterization of the interaction of the δ and α subunits of the *Escherichia coli* F_1F_o-ATP synthase by NMR spectroscopy. *Biochemistry* 44:11786–94
90. Rees DM, Leslie AG, Walker JE. 2009. The structure of the membrane-extrinsic region of bovine ATP synthase. *PNAS* 106:21597–601
91. Hohmann-Marriott MF, Blankenship RE. 2011. Evolution of photosynthesis. *Annu. Rev. Plant Biol.* 62:515–48
92. Rand DM, Haney RA, Fry AJ. 2004. Cytonuclear coevolution: the genomics of cooperation. *Trends Ecol. Evol.* 19:645–53
93. Lau WC, Rubinstein JL. 2012. Subnanometre-resolution structure of the intact *Thermus thermophilus* H^+-driven ATP synthase. *Nature* 481:214–18
94. Dautant A, Meier T, Hahn A, Tribouillard-Tanvier D, di Rago JP, Kucharczyk R. 2018. ATP synthase diseases of mitochondrial genetic origin. *Front. Physiol.* 9:329
95. He J, Ford HC, Carroll J, Douglas C, Gonzales E, et al. 2018. Assembly of the membrane domain of ATP synthase in human mitochondria. *PNAS* 115:2988–93
96. Pullman ME, Monroy GC. 1963. A naturally occurring inhibitor of mitochondrial adenosine triphosphatase. *J. Biol. Chem.* 238:3762–69
97. Bason JV, Montgomery MG, Leslie AG, Walker JE. 2014. Pathway of binding of the intrinsically disordered mitochondrial inhibitor protein to F_1-ATPase. *PNAS* 111:11305–10
98. Gledhill JR, Montgomery MG, Leslie AG, Walker JE. 2007. How the regulatory protein, IF_1, inhibits F_1-ATPase from bovine mitochondria. *PNAS* 104:15671–76
99. Cabezon E, Montgomery MG, Leslie AGW, Walker JE. 2003. The structure of bovine F_1-ATPase in complex with its regulatory protein IF1. *Nat. Struct. Biol.* 10:744–50
100. Cabezon E, Arechaga I, Butler PJG, Walker JE. 2000. Dimerization of bovine F_1-ATPase by binding the inhibitor protein, IF1. *J. Biol. Chem.* 275:28353–55
101. Tanigawara M, Tabata KV, Ito Y, Ito J, Watanabe R, et al. 2012. Role of the DELSEED loop in torque transmission of F_1-ATPase. *Biophys. J.* 103:970–78
102. Junesch U, Gräber P. 1987. Influence of the redox state and the activation of the chloroplast ATP synthase on proton-transport-coupled ATP synthesis hydrolysis. *Biochim. Biophys. Acta* 893:275–88
103. Nalin CM, McCarty RE. 1984. Role of a disulfide bond in the gamma subunit in activation of the ATPase of chloroplast coupling factor 1. *J. Biol. Chem.* 259:7275–80
104. Bernardi P, Di Lisa F. 2015. The mitochondrial permeability transition pore: molecular nature and role as a target in cardioprotection. *J. Mol. Cell Cardiol.* 78:100–6

105. Watt IN, Montgomery MG, Runswick MJ, Leslie AG, Walker JE. 2010. Bioenergetic cost of making an adenosine triphosphate molecule in animal mitochondria. *PNAS* 107:16823–27
106. Saroussi S, Schushan M, Ben-Tal N, Junge W, Nelson N. 2012. Structure and flexibility of the C-ring in the electromotor of rotary F_OF_1-ATPase of pea chloroplasts. *PLOS ONE* 7:e43045
107. Pogoryelov D, Yu J, Meier T, Vonck J, Dimroth P, Müller DJ. 2005. The c_{15} ring of the *Spirulina platensis* F-ATP synthase: F_1/F_o symmetry mismatch is not obligatory. *EMBO Rep*. 6:1040–44
108. Pogoryelov D, Yildiz Ö, Faraldo-Gomez JD, Meier T. 2009. High-resolution structure of the rotor ring of a proton-dependent ATP synthase. *Nat. Struct. Mol. Biol.* 16:1068–73
109. Schulz S, Wilkes M, Mills DJ, Kühlbrandt W, Meier T. 2017. Molecular architecture of the N-type ATPase rotor ring from *Burkholderia pseudomallei*. *EMBO Rep*. 18:526–35
110. Murata T, Yamato I, Kakinuma Y, Leslie AG, Walker JE. 2005. Structure of the rotor of the V-type Na^+-ATPase from *Enterococcus hirae*. *Science* 308:654–59
111. Pogoryelov D, Klyszejko AL, Krasnoselska GO, Heller EM, Leone V, et al. 2012. Engineering rotor ring stoichiometries in the ATP synthase. *PNAS* 109:E1599–608
112. Preiss L, Klyszejko AL, Hicks DB, Liu J, Fackelmayer OJ, et al. 2013. The c-ring stoichiometry of ATP synthase is adapted to cell physiological requirements of alkaliphilic *Bacillus pseudofirmus* OF4. *PNAS* 110:7874–79
113. Vonck J, Krug von Nidda T, Meier T, Matthey U, Mills DJ, et al. 2002. Molecular architecture of the undecameric rotor of a bacterial Na^+-ATP synthase. *J. Mol. Biol.* 321:307–16
114. Dibrova DV, Galperin MY, Mulkidjanian AY. 2010. Characterization of the N-ATPase, a distinct, laterally transferred Na^+-translocating form of the bacterial F-type membrane ATPase. *Bioinformatics* 26:1473–76
115. Zhao J, Benlekbir S, Rubinstein JL. 2015. Electron cryomicroscopy observation of rotational states in a eukaryotic V-ATPase. *Nature* 521:241–45
116. Mazhab-Jafari MT, Rohou A, Schmidt C, Bueler SA, Benlekbir S, et al. 2016. Atomic model for the membrane-embedded V_o motor of a eukaryotic V-ATPase. *Nature* 539:118–22
117. Kühlbrandt W, Davies KM. 2016. Rotary ATPases: a new twist to an ancient machine. *Trends Biochem. Sci.* 41:106–16
118. Cain BD, Simoni RD. 1986. Impaired proton conductivity resulting from mutations in the *a* subunit of F_1F_o ATPase in *Escherichia coli*. *J. Biol. Chem*. 261:10043–50
119. Ho BK, Gruswitz F. 2008. HOLLOW: generating accurate representations of channel and interior surfaces in molecular structures. *BMC Struct. Biol.* 8:49
120. Vik SB, Antonio BJ. 1994. A mechanism of proton translocation by F_1F_o ATP synthases suggested by double mutants of the *a* subunit. *J. Biol. Chem.* 269:30364–69
121. Allegretti M, Mills DJ, McMullan G, Kühlbrandt W, Vonck J. 2014. Atomic model of the F_{420}-reducing [NiFe] hydrogenase by electron cryo-microscopy using a direct electron detector. *eLife* 3:e01963
122. Bartesaghi A, Matthies D, Banerjee S, Merk A, Subramaniam S. 2014. Structure of β-galactosidase at 3.2-Å resolution obtained by cryo-electron microscopy. *PNAS* 111:11709–14
123. Preiss L, Yildiz Ö, Hicks DB, Krulwich TA, Meier T. 2010. A new type of proton coordination in an F_1F_o-ATP synthase rotor ring. *PLOS Biol.* 8:e1000443
124. Symersky J, Pagadala V, Osowski D, Krah A, Meier T, et al. 2012. Structure of the c_{10} ring of the yeast mitochondrial ATP synthase in the open conformation. *Nat. Struct. Mol. Biol.* 19:485–91
125. Pogoryelov D, Krah A, Langer JD, Yildiz Ö, Faraldo-Gomez JD, Meier T. 2010. Microscopic rotary mechanism of ion translocation in the F_o complex of ATP synthases. *Nat. Chem. Biol.* 6:891–99
126. Mitchell P. 2011. Chemiosmotic coupling in oxidative and photosynthetic phosphorylation. *Biochim. Biophys. Acta* 1807:1507–38
127. Junesch U, Gräber P. 1991. The rate of ATP-synthesis as a function of ΔpH and Δψ catalyzed by the active, reduced H^+-ATPase from chloroplasts. *FEBS Lett*. 294:275–78
128. Cruz JA, Sacksteder CA, Kanazawa A, Kramer DM. 2001. Contribution of electric field (Δψ) to steady-state transthylakoid proton motive force (*pmf*) in vitro and in vivo. Control of *pmf* parsing into Δψ and ΔpH by ionic strength. *Biochemistry* 40:1226–37

129. Schutz CN, Warshel A. 2001. What are the dielectric "constants" of proteins and how to validate electrostatic models? *Proteins* 44:400–17
130. Gilson MK, Honig BH. 1986. The dielectric constant of a folded protein. *Biopolymers* 25:2097–119
131. Kinosita K, Yasuda R, Noji H, Adachi K. 2000. A rotary molecular motor that can work at near 100% efficiency. *Philos. Trans. R. Soc. B* 355:473–89
132. Pänke O, Cherepanov DA, Gumbiowski K, Engelbrecht S, Junge W. 2001. Viscoelastic dynamics of actin filaments coupled to rotary F-ATPase: angular torque profile of the enzyme. *Biophys. J.* 81:1220–33
133. Spetzler D, York J, Daniel D, Fromme R, Lowry D, Frasch W. 2006. Microsecond time scale rotation measurements of single F_1-ATPase molecules. *Biochemistry* 45:3117–24
134. Miller JH Jr., Rajapakshe KI, Infante HL, Claycomb JR. 2013. Electric field driven torque in ATP synthase. *PLOS ONE* 8:e74978
135. Junge W, Lill H, Engelbrecht S. 1997. ATP synthase: an electrochemical transducer with rotatory mechanics. *Trends Biochem. Sci.* 22:420–23
136. Baker LA, Watt IN, Runswick MJ, Walker JE, Rubinstein JL. 2012. Arrangement of subunits in intact mammalian mitochondrial ATP synthase determined by cryo-EM. *PNAS* 109:11675–80
137. Jiko C, Davies KM, Shinzawa-Itoh K, Tani K, Maeda S, et al. 2015. Bovine F_1F_o ATP synthase monomers bend the lipid bilayer in 2D membrane crystals. *eLife* 4:e06119
138. Anselmi C, Davies KM, Faraldo-Gomez JD. 2018. Mitochondrial ATP synthase dimers spontaneously associate due to a long-range membrane-induced force. *J. Gen. Physiol.* 150:763–70
139. Brandt T, Mourier A, Tain LS, Partridge L, Larsson NG, Kühlbrandt W. 2017. Changes of mitochondrial ultrastructure and function during ageing in mice and *Drosophila*. *eLife* 6:e24662
140. Bornhövd C, Vogel F, Neupert W, Reichert AS. 2006. Mitochondrial membrane potential is dependent on the oligomeric state of F_1F_o-ATP synthase supracomplexes. *J. Biol. Chem.* 281:13990–98
141. Saddar S, Dienhart MK, Stuart RA. 2008. The F_1F_o-ATP synthase complex influences the assembly state of the cytochrome *bc1*-cytochrome oxidase supercomplex and its association with the TIM23 machinery. *J. Biol. Chem.* 283:6677–86
142. Davies KM, Blum TB, Kühlbrandt W. 2018. Conserved in situ arrangement of complex I and III_2 in mitochondrial respiratory chain supercomplexes of mammals, yeast, and plants. *PNAS* 115:3024–29
143. Rieger B, Junge W, Busch KB. 2014. Lateral pH gradient between OXPHOS complex IV and F_0F_1 ATP-synthase in folded mitochondrial membranes. *Nat. Commun.* 5:3103
144. Llopis J, McCaffery JM, Miyawaki A, Farquhar MG, Tsien RY. 1998. Measurement of cytosolic, mitochondrial, and Golgi pH in single living cells with green fluorescent proteins. *PNAS* 95:6803–8
145. Teixeira FK, Sanchez CG, Hurd TR, Seifert JRK, Czech B, et al. 2015. ATP synthase promotes germ cell differentiation independent of oxidative phosphorylation. *Nat. Cell Biol.* 17:689–96
146. Preiss L, Langer JD, Yildiz Ö, Eckhardt-Strelau L, Guillemont JEG, et al. 2015. Structure of the mycobacterial ATP synthase F_o rotor ring in complex with the anti-TB drug bedaquiline. *Sci. Adv.* 1:e1500106
147. Rühle T, Leister D. 2015. Assembly of F_1F_o-ATP synthases. *Biochim. Biophys. Acta* 1847:849–60
148. Stoldt S, Wenzel D, Kehrein K, Riedel D, Ott M, Jakobs S. 2018. Spatial orchestration of mitochondrial translation and OXPHOS complex assembly. *Nat. Cell Biol.* 20:528–34
149. Sousa FL, Nelson-Sathi S, Martin WF. 2016. One step beyond a ribosome: the ancient anaerobic core. *Biochim. Biophys. Acta* 1857:1027–38
150. Nelson N. 1992. Evolution of organellar proton-ATPases. *Biochim. Biophys. Acta* 1100:109–24
151. Mulkidjanian AY, Makarova KS, Galperin MY, Koonin EV. 2007. Inventing the dynamo machine: the evolution of the F-type and V-type ATPases. *Nat. Rev. Microbiol.* 5:892–99
152. Preiss L, Langer JD, Hicks DB, Liu J, Yildiz Ö, et al. 2014. The *c*-ring ion binding site of the ATP synthase from *Bacillus pseudofirmus* OF4 is adapted to alkaliphilic lifestyle. *Mol. Microbiol.* 92:973–84